NTNU

Norwegian University of
Science and Technology

A numerical investigation of strain-softening in soft clay for a modelled shear vane

Olav Henneseid

Geotechnics and Geohazards
Submission date: June 2018
Supervisor: Gustav Grimstad, IBM

Norwegian University of Science and Technology
Department of Civil and Environmental Engineering

NORGES TEKNISK-
NATURVITENSKAPELIGE UNIVERSITET
INSTITUTT FOR BYGG OG MILJØTEKNIKK

Report Title:	Date: **11.06.2018**	
A numerical investigation of strain-softening in soft clay for a modelled shear vane	Number of page (incl. appendices): **67**	
	Master Thesis	**x**
Name: **Olav Henneseid**		
Professor in charge/supervisor: **Gustav Grimstad**		
Other external professional contacts/supervisors:		

Extract:

The strain-softening phenomenon has been extensively studied the last decades in context of numerical modelling and progressive failure mechanism. In this study, a vane is modelled in soft clay with a negative dilatancy. The vane is applied several deformation rates which results in different strain-softening patterns.

It is of interest to investigate the interactive connection between shear band formation and local drainage mechanics in FEM for different mesh qualities. A setup of four different mesh qualities are kept consistent for all cases. Coarse, medium, fine and very fine mesh refinements of 326, 520, 1400, 4186 elements are used. Consolidation analysis are carried out in Plaxis 2d with different time-steps. The shear band thickness is an important parameter as it explains the strain-level and consolidation rate. Plaxis displays issues regarding objective shear band thicknesses and leaves these as undetermined values. Consequently, results are sensitive to the element size of the mesh. Hence, mesh dependency must be achieved to get objective results in terms of shear band formations and peak-strength.

Using the conventional Hardening soil model in Plaxis 2d resulted in increasing peak-values for slower deformation rates. Hardening soil model appeared rate-independent and insufficient for the aim of this thesis. Afterwards, a rate-dependent user designed soil model called "Unified enhanced soft soil creep model" were used to obtain adequate results. Results indicated rate-dependency as faster rates resulted in higher peak-values with steeper decrease to a lower residual strength. It was observed zones of suction behind each vane blade with maximum values of 60-80 kPa indicating a lack of tension cut-off criterion for the user-designed soil model.

It is concluded in this study that both Hardening soil and Unified enhanced soft soil creep model could not generate mesh-dependent results for a soft contractive clay.

Keywords:

1. Strain-softening
2. Mesh-dependency
3. Shear vane
4. Plaxis 2d

Acknowledgement

This thesis represents the end of two years of hard work. It has been frustrating and difficult sometimes, but the accomplishments of understanding through hard work has made it worth it. I would like to thank my supervisor Gustav Grimstad for always being available with proper guidance through the whole period. I would also like to thank everyone in the geotechnical department at NTNU that was involved in this study. Thanks to my family and friends for supporting me throughout my stay in Trondheim.

Abstract

Plaxis 2d is used to model a shear vane investigation in soft clay with negative dilatancy. Behaviour of sensitive clay and strain-softening is elaborated in theoretical overview. Chapter 3 provides information of the subjective event of mesh refinement in Plaxis which affects the results and generates non-unique answers for consolidation calculations. The conventional Hardening soil model and the user-designed "Unified enhanced soft soil creep model" were used in this analysis. Drainage effects across emerged shear bands were studied for both soil models which resulted in a Gaussian curve, where maximum excessive pore pressure build-up were located in the shear band centre. Pore pressure gradually decreases as drainage from the shear band continues post-failure. This process showed to be mesh-dependent for both soil models. Simulations with Hardening soil resulted in rate-independent characteristics, where slower deformation rates gave higher peak-strengths compared to faster rates with lower peak-strengths. "Unified enhanced soft soil creep model" were used, and generated rate-dependant results, where faster rates gave higher peak-values, but lower residual strengths. Also, the emerged shear band in Plaxis were observed to be of a rounded-square shape rather than perfect circular. Results with the rate-dependant soil model gave answers that were more similar upon mesh refinements compared to hardening soil. It is concluded that there could not be found any mesh-independent results by comparing a consistent deformation rate with 4 mesh refinements for both soil models.

Sammendrag

I dette studiet er FEM-programmet Plaxis 2d benyttet for å modellere et vingeborforsøk i en kontraktant og sensitiv leire. Egenskaper for en sensitive leire er utdypet i andre kapittel. I kapittel 3 er det en redegjørelse av hvorvidt personavhengige avgjørelser av mesh-kvaliteten bestemmer utfallet av analysene i Plaxis. I dette studiet har det blitt brukt to forksjellige jordmodeller, Hardening soil og en brukerdesignet modell kalt "Unified enhanced soft soil creep model". Resultater fra Hardening soil viste seg å være rateuavhengig da tregere deformasjonsrater ga høyere maksimal styrke. Dermed ble jordmodellen "Unified enhanced soft soil creep model" benyttet. Resultatene viste til et rateavhengig forløp hvor nå raskere rater ga høyere maksimal motstand med lavere residual styrke. Resultatene viste også mindre avvik fra hverandre ved sammenligning av flere mesh i forhold til Hardening soil. Denne studien konkluderer med at jordmodellene som ble benyttet ikke kunne generere meshuavhengige og unike resultater

Contents

Chapter 1

Introduction

This chapter is presented to describe the background and aim for the master thesis.

1.1 Background

Most soft sensitive clays exhibit a strain-softening material behaviour. Strain-softening response can affect soil stability and is therefor an important subject in geotechnical engineering. This phenomenon have been studied the last decades in context of numerical modelling and progressive slope failure. Slope failure in soft clay deposits can be initiated in a progressive manner where shear mobilization along a slip surface varies. Progressive failures are complicated because each slide event is unique and can combine several mechanisms. Based on Kalsrud et al. [1], there can be identified four different modes;

- Downward progressive failure
- Retrogressive failure
- Upward progressive failure
- Lateral spread

The first two modes are typical in Norway, and can be challenging to simulate since LEM no longer is valid. However, FEM is a well suited method to deal with the complexity of this matter. In order to analyze the progressive failure phenomenon, strain-softening material behaviour should be considered. Today, most elasto-plastic soil models are not adequate in analysis where strain-softening behaviour is considerable. In a finite element analysis, the strain-softening behaviour requires knowledge of soil parameters like permeability and viscosity, shear band thickness and deformation rates. For geotechnical engineering, its of great importance to develop soil models that can be used to gain accurate and objective estimations of actual situations.

1.2 Aim

The aim for this thesis is to achieve mesh dependency for a shear vane modelled in Plaxis 2D. The thickness of an arbitrary shear band is a decisive factor as narrower shear bands will drain faster. This implies that there can be a situation when internal drainage balances the softening process for a prescribed deformation rate, and establishes a steady state situation. If this is achieved, the shear band thickness becomes unique and mesh independent.

1.3 Software

For the numerical analysis, a FEM software called Plaxis 2D has been used to collect data. Plaxis is a finite element analysis software developed by Plaxis Company. Plaxis is created in a cooperation with several universities around the world including Delft University of Technology in Netherlands and NTNU in Norway. Plaxis is a phase-based finite element software, which is designed primarily for geotechnical problems. Plaxis is a convenient tool to use, especially since there are several soil models such as Mohr-Coulomb, Hardening soil, Modified Cam-Clay as well as user-designed models.

1.4 Structure of the Thesis

The thesis is divided into 5 chapters:

- Chapter 1
  The first chapter, which will explain the background and aim for this thesis, as well as the chosen FEM software.

- Chapter 2
  Provides a qualitative overview of previous and relevant work, with an elaboration of classical consolidation theory which Plaxis is based on.

- Chapter 3
  This chapter introduces the approach in Plaxis 2D, assumptions and clarifications as well as the chosen soil models and parameters. There is also a brief discussion about mesh dependency.

- Chapter 4
  The results from Plaxis can be found in this chapter for both soil models. This chapter includes excess pore pressure distribution and torque-strength upon several deformation rates.

- Chapter 5
  The last chapter. Summarizes the study by discussing the results followed by a conclusion.

Chapter 2

Theoretical overview

In this chapter, a theoretical overview of previous relevant work is introduced.

2.1 Soft sensitive clay

Soft sensitive clay is a term used to characterize marine clay deposits which were located in saltwater during the last glaciation of Scandinavia around 10 000 years ago. The electrically charged clay minerals then attached themselves to the chloride ions. Melting of the ice led to an uplift where some clay deposits were lifted over sea level. In some locations, years of infiltration of fresh water in marine clays have washed out the salt ions. Consequently, there can be located clay deposits today which have an open soil structure with little bonds. This results in a clay that exhibits same strength, but acts unstable to external disturbances and will collapse and loose resistance as soon as an external load goes beyond maximum strength.

In terms of sensitivity, different types of clay can be classified from its strength attributes. The sensitivity is given as a ratio of undisturbed strength (s_u) and remoulded strength (s_{ur}) which is an attainable parameter by performing a shear vane test.

$$s_t = \frac{s_u}{s_{ur}} \tag{2.1}$$

This ratio was defined by Terzaghi in 1944 [2], and can help differentiate between soft and firm clay deposits.

Clay	S_t (-)
Less sensitive	< 8
Medium sensitive	$8 - 30$
Highly sensitive	> 30

Table 2.1: Sensitivity classification

Table 2.1 displays limit values that can contribute to classify clays according to the Norwegian Public Roads Administration [3]. In Norwegian practice, clays that surpasses a s_t ratio of 30 is considered a highly sensitive clay. In addition, quick clays are identified with a remoulded shear strength of $< 0,5$ kN/m^3, and can appear practically as a fluid.

Naturally, most clays will lose some of the strength when remoulded, but the strength loss varies. The remoulded strength of clays are strongly related to current water content and previous consolidation stresses. Clays that have been heavily over-consolidated are considered insensitive ($S_t < 8$), where a normally consolidated clay is commonly considered in the medium sensitivity range ($8 < S_t < 30$).

Shear strength values can contribute to describe the firmness of clays. According to Norwegian Public Roads Administration [3], soft clays have shear strengths lower than 25 kN/m^2 as indicated in Table 2.2 below.

Clay	S_u (kN/m^2)
Soft	< 25
Medium	$25 - 50$
Firm	> 50

Table 2.2: Shear strengths for clays.

2.1.1 Dilatancy

Soils subjected to shear stress behaves differently than other materials as drained soils will change in volume and undrained soils generates excess pore pressure. This soil behaviour initiates due to dilatancy. If there is a pore pressure build up while shearing, the soil is contracting or in other words dilating negatively. When applying shear strain, dilatancy can be understood as the soil particle reorientation illustrated in Figure 2.1 below.

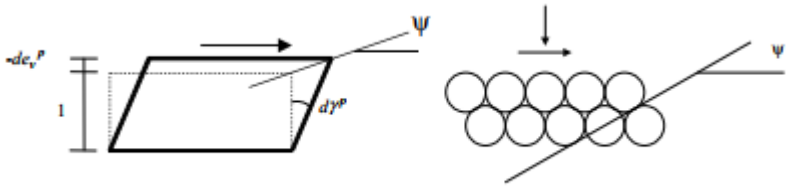

Figure 2.1: Illustration of shear strain and dilatancy[4]

The rearrangement of the soil particles requires several particles to climb over one another contributing to the frictional resistance. The volume increase which is caused by particles moving is given by the angle of dilatancy (Ψ) illustrated in Figure 2.1. The angle of dilatancy is much lower than the friction angle (ϕ), usually only a few degrees. A distinct feature for over consolidated clays, is that Ψ is dependant of the overconsolidation ratio(OCR). High OCR typically shows a volume expansion while lower OCR results in a volume contraction [5]. Sensitive or quick clay tend to behave contractant which implies a negative Ψ.

2.1.2 Strain-softening behaviour

As many other geomaterials, sensitive clays tend to follow a strain rate dependent behavior [6][7]. This means that clays can exhibit different peak-strength values due to viscosity, permeability and drainage from the shear band for different rates of deformation. Post-peak strength response for soft clays displays a gradual strength reduction during undrained shearing. This phenomenon is associated with material softening, and often referred to as

strain-softening. For undrained shearing, there is no volumetric change and the contractancy will cause generation of excess pore pressure. The reduction in effective stress leads to a gradual reduction of shear strength as pore pressure dissipates.

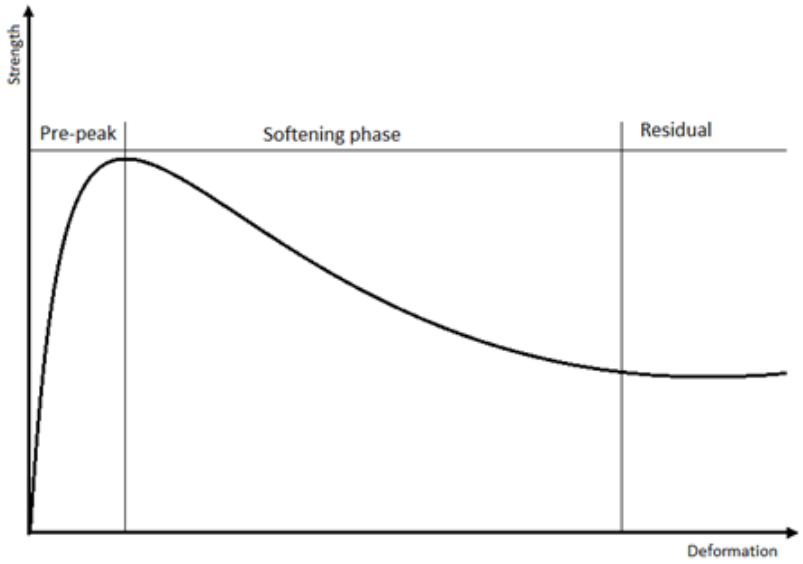

Figure 2.2: An idealized undrained strength-deformation curve for a soft sensitive clay.

Figure 2.2 shows an idealized graph of a strength-deformation relation for a sensitive, contracting clay. Strain-softening can be characterized by three phases. From the figure it is notable that the pre-peak phase is relatively short and will end as soon as global peak-strength value is reached. Afterwards, the softening phase will initiate and strength will gradually reduce to a residual state. Residual phase is achieved when the generation of pore pressure has reached its limits in terms of porosity, and that all excess pore water has dissipated. Residual and peak-strength of the same clay sample can vary. Under rapid loading, pore pressure is high and confined to a narrow area. For slower rates, the pore pressure spreads over a larger volume, implying a lower pore pressure build up. In other words, its reasonable to assume the residual strength is rate-dependent. Such behavior of soft sensitive clay is consistent with the experimental work of Bernander and Svensk [8] and Bernander et al. [9], on soft Swedish clay as well as the numerical work done by Jostad et al. [10] and Thakur [11] regarding their analysis of

strain localization on sensitive clays.

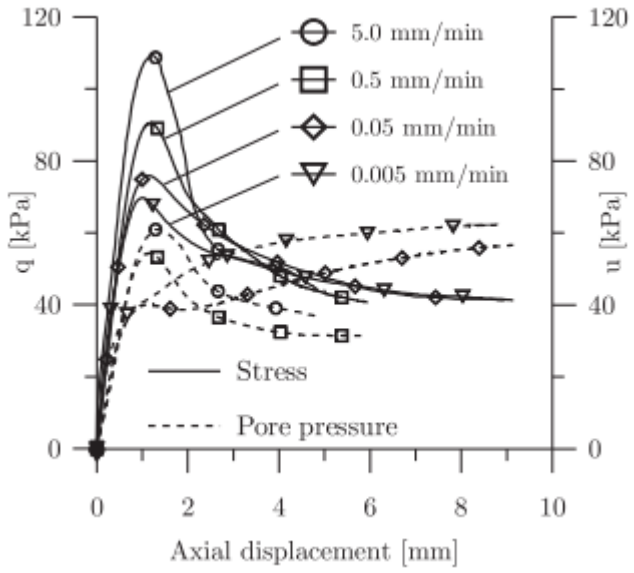

Figure 2.3: Several rates with corresponding softening tendencies in a triaxial test. (From Gylland [12]).

Figure 2.3 illustrates experimental results from a Norwegian quick clay. A modified triaxial apparatus with four different rates of axial displacement were used to observe post-peak material behaviour. It can be seen that increased rates will result in higher peak resistance, but steeper softening response due to pore pressure build-up.

Friction and cohesion softening can also contribute to the strain-softening phenomenon. After the pioneering work of Skempton [13], a gradual decrease of both friction angle (ϕ) and cohesion (c) is associated with softening response in OC clay illustrated in Figure 2.4. Previous research from Burland et al. [14] and Vermeer et al. [15] have shown that the decrease to residual state for ϕ is much lower than for c, which means that cohesion softening is considered more dramatic than friction softening.

Janbu [16] suggested that for soft sensitive clays, the effective strength parameters ϕ and c are independent whether a clay is loaded under undrained or drained condition and if the load subjected clay is at its peak or post-peak

state. Several studies have been done (e.g Bernander [17] and Jostad et al. [10]) which proves that shear strength softening in soft sensitive clay is governed by shear induced pore pressure instead of friction or cohesion softening. However, strength reduction for both ϕ and c have been observed by Stark and Contreas [18] for strain levels up to 10-20 % for a constant volume ring shear test on a low sensitive plastic Drammen clay.

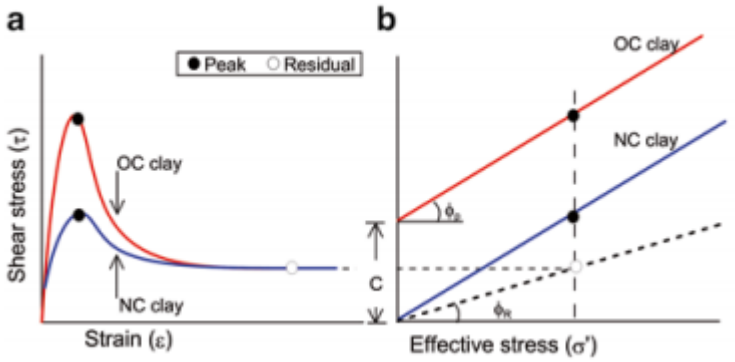

Figure 2.4: Strain softening for NC and OC clay under drained conditions: (**a**) shear stress-strain relation, (**b**) Corresponding softening for ϕ and c. (After Skempton [13])

2.1.3 Shear bands

Shear band formation is associated with material instability and can occur when applying shear strain on a clay sample. As strain increases towards yield state of the clay, all further strain tend to concentrate in narrow zones. These narrow zones can often be referred to as shear bands, failure surfaces or slip surfaces which is often used for drained conditions. A shear band can be defined as a zone where plastic strain occur with an elastically unloading outside soil body. Shear bands usually develops within a broad range of ductile materials such as metals, plastic, granular materials and soils.

The shear band phenomenon is an important subject in engineering as it precedes failure mechanisms. The thickness of a shear band is a significant parameter to achieve in context of strain-softening mechanics, but complex to anticipate. It is well-known that the shear band width of granular materials

is determined by the grain size [19]. However, in soft sensitive clay under globally undrained conditions, publications (Jostad [10] and Thakur [11]) have demonstrated that the shear band thickness in early stages of soil failure is governed by the deformation rate. Under undrained conditions the rate of deformation affects the local drainage from the shear bands. A thinner shear band will possess a higher level of strain compared to a wider discontinuity. Consequently, a narrow shear band formation will result in a larger reduction of shear resistance in the post-peak regime. Hence, the decrease in strength after post-peak is related to the rate of deformation [20], which can be seen from Figure 2.3.

Figure 2.5: Observable shear band in a modified triaxial cell[12]

Shear bands are often in μm-scale, which makes it difficult to inspect without a microscope. However, from Figure 2.5 it can easily be observed. The clay sample in the modified triaxial apparatus (same apparatus as discussed in Section 2.1.2) are confined in a membrane that makes the structure of the shear band visible.

2.2 Shear vane

The shear vane is one of the most common in-situ investigation method for estimating undrained shear strengths of cohesive soils, mainly clays and silty clays. A shear vane test is often preferred as it is easy to use and a cost-effective alternative. A conventional vane has a ratio $H/D = 2$, where a small vane is considered $55 \cdot 110$ mm (recommended for $S_{uv} = 30 - 100$ kN/m^3) and big vane is $65 \cdot 130$ mm ($S_{uv} < 50$ kN/m^3), illustrated in Figure 2.6. The shear vane can be operated manually or by an electrical device.

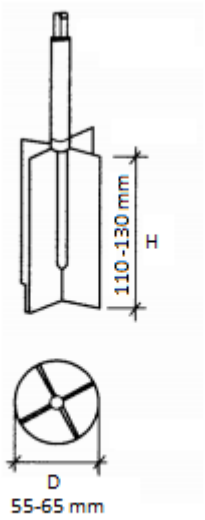

Figure 2.6: Illustration of the shear vane[21].

The testing procedure is done by vertically forcing the shear vane into the soil at a desired depth and then rotated at a slow rate of 6° or 12° per minute towards failure while measuring the torque. Usually, the rotation is continued after shearing to measure remoulded shear strength. This is done to obtain the sensitivity parameter, S_t. Since it can be presumed a circular failure mechanism, its possible to use the torque to calculate the shear strength of the soil:

$$S_{uv} = \frac{6}{7}\frac{T}{\pi D^3} \tag{2.2}$$

Where;
T = torque
D = diameter

When inserting the vane, care has to be taken so that the vane will not disturb the soil and generate excess pore pressure, resulting in less resistance. Use of a shear vane also requires knowledge of the soil strata. Results should be thoroughly controlled, as this intuitive investigation needs to be carried out carefully, especially if operated manually.

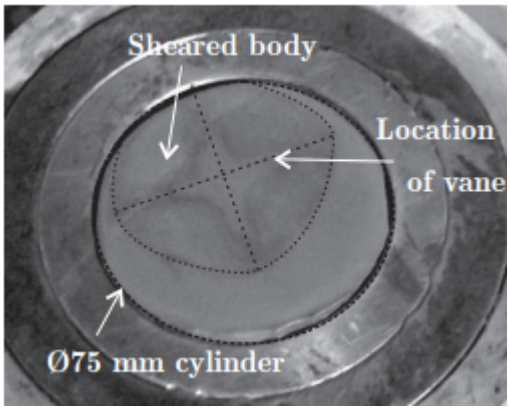

Figure 2.7: Over-cored clay sample after vane investigation. [12]

An example of emerged shear zones from a vane investigation, is illustrated by a Ø75 mm over-cored clay sample in Figure 2.7. It can be observed that the outline of sheared zones are of a more well-rounded square shape instead of a perfect circular shape.

2.3 One dimensional consolidation

The mechanics of dissipation and generation of pore pressure from the shear band can be derived from the continuity rule which Plaxis is based upon. For a continuity condition the principle is that the amount of outflow of pore water is related to the volume change. Mathematically, the continuity condition can be described as:

$$\frac{\delta \nu}{\delta z} = \frac{\delta \epsilon}{\delta t} \tag{2.3}$$

Where;
ν = flow rate
z = depth
ϵ = strain
t = time

Using Darcy's law to define the flow rate (ν) and the constitutive model for the strain (ϵ), the expression for the continuity condition can be a differential equation:

$$c_v \cdot \frac{\delta^2 u}{\delta z^2} = \frac{\delta u}{\delta t} \tag{2.4}$$

Where;
u = pore pressure
c_v = vertical coefficient of consolidation

The expression of consolidation theory in analytically form were given first by Terzaghi in 1923. The expression was made to predict the progress of settlement in uniformly loaded clay layers. Through the years, Terzaghi's consolidation theory has been extended to take account for non-linear behavior and other effects associated with large strains and deformations.

Chapter 3

Modelling with FEM

The approach and assumptions done through the modelling phase of this thesis is clarified in this section.

3.1 Mesh dependency

The finite element method is a popular tool for modelling strain-softening related issues, as it is possible to receive results from complex geometry with interactive non-linear material response. However, there are some difficulties with this type of modelling that is worth mentioning. Plaxis is based on classical continuity theory, and for strain-based modelling in Plaxis, the amount of strain that develops in the shear band will decide the global response. This value is accordingly given by the shear band thickness, which Plaxis leaves as an undetermined value. Upon material instability the problem becomes ill-posed as the governing differential equations loose ellipticity [11]. Consequently, the mesh will act as an internal length parameter and the shear band thickness takes the minimum size possible [22], [23]. In other words, the results will suffer from mesh dependency and generate non-unique answers which can be seen in Figure 3.1 for a DSS test in Plaxis 2D with different mesh qualities.

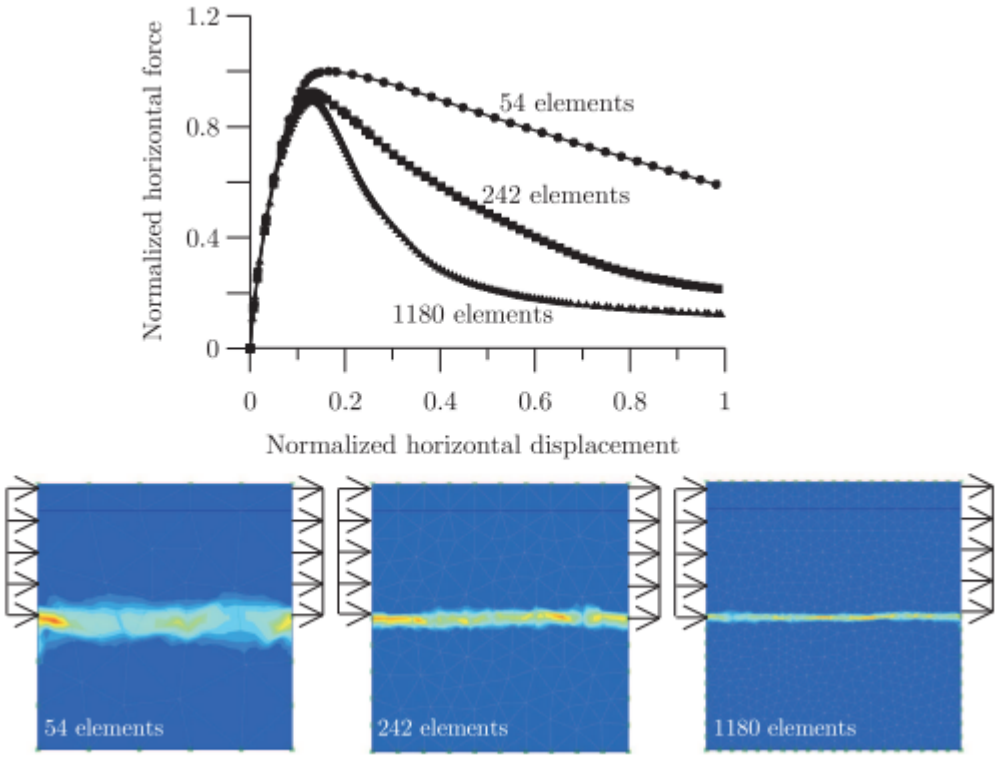

Figure 3.1: Strength-displacement relation for different mesh refinements. [12].

Notably, it exists several techniques to obtain mesh independent solutions which are often referred to as regularization techniques. These are techniques that are based on making additional mathematical formulations to avoid FEM to set the mesh as an internal length parameter. This can be done by directly inserting a shear band thickness or indirectly through parameters like viscosity and permeability. Additionally for continuum based modelling, there is a need for having element size smaller than shear band thickness, which for soft clays requires an extremely fine mesh [12].

3.2 Modelling approach

A simple quadratic plain strain model is made in Plaxis 2D, which is to simulate a shear vane in a planar perspective. Overview of the model can be seen in Figure 3.2 below. In this thesis, a conventional small vane size has been modelled, implying a diameter of 55 mm and height of 110 mm to interpret the torque.

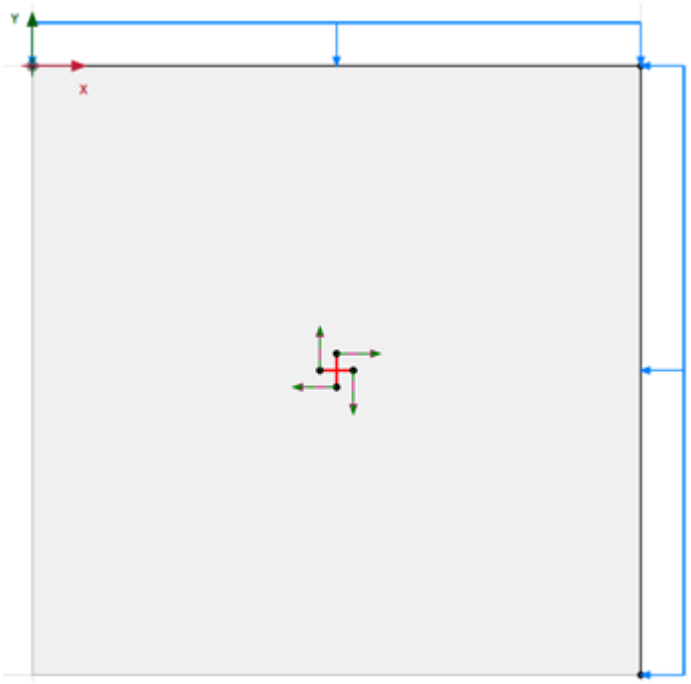

Figure 3.2: FE model of the shear vane.

The boundary conditions are set to horizontally fixed and vertically fixed to the X_{min} and Y_{min} axis, respectively. The stress induced boundaries (X_{max} and Y_{max}) are set to respond free to deformation. Zero-thickness plates with high stiffness have been used to create the vane. Rotation of the shear vane is made by a prescribed point deformation at the tip of each vane blade. Since this model is made to neglect the gravitational contribution along the y-axis, unit weight of the soil (γ) is set 0 kN/m^3. Hence, the stress condition in the soil is defined by the external load ($\Delta\sigma_x, \Delta\sigma_y$), which is set to a uniform value of 100 kPa. Several mesh densities are created to compare output from Plaxis.

In this analysis, consistent mesh refinements of 4186, 1400, 520, 326 elements with 15-noded triangular element setting is used for the calculations. The different meshes were made by increasing the coarseness factor from 0.03125 (most optimal mesh possible) to 0.04419. The four different meshes can be seen from very fine to coarse quality in Figure 3.3.

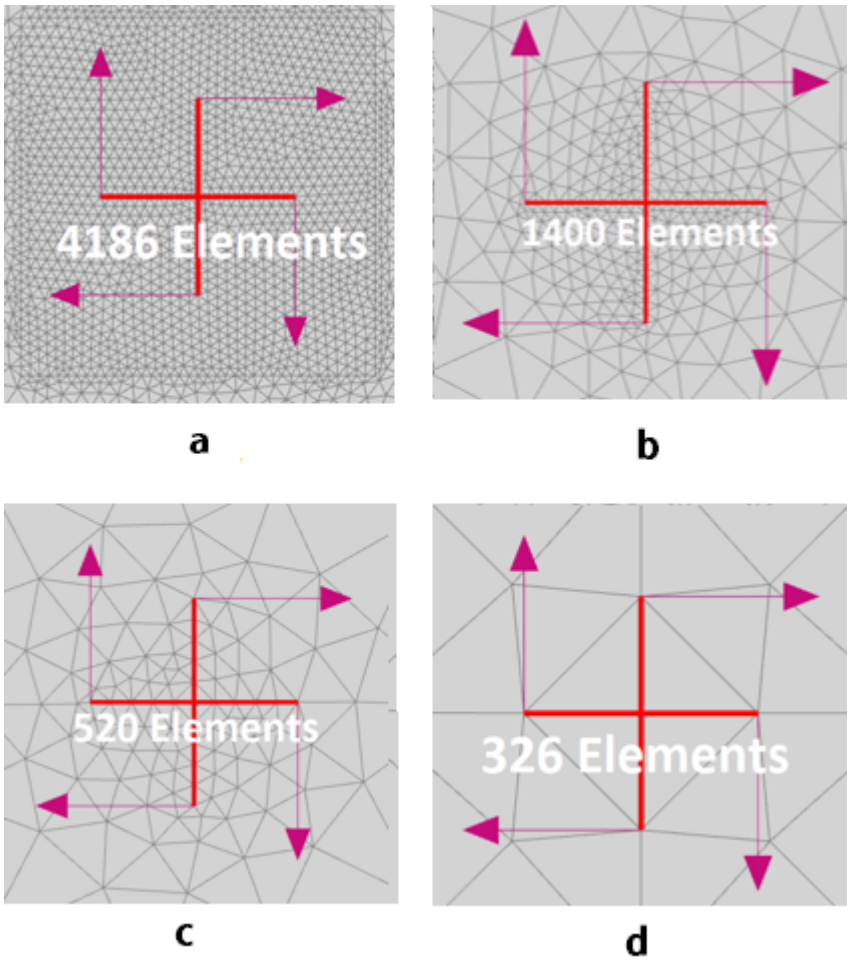

Figure 3.3: Mesh refinements of: (**a**) 4186 elements, (**b**) 1400 elements, (**c**) 520 elements, (**d**) 326 elements.

Calculations are done through three different phases, initial phase exclusively. During the first phase, all boundary conditions and external load is activated, and the calculation is done by ignoring undrained behaviour. In addition, an elastic soil material was made to achieve the correct stress condition in the soil. This was done by changing the Poisson's ratio (ν) to 0.5. The original soil model is then replaced at the second phase, where also the plates are activated and displacements are reset to zero. The third and last phase is where the prescribed deformations are activated and calculation type is changed from plastic to consolidation analysis. Tolerated error has been kept at a default value of 0.01 through a 100 step calculation. The modelled vane is applied up to 8 prescribed deformation rates for both soil models, which are kept permanent for all of the calculations. This has been done by increasing time steps with a constant prescribed deformation of 5 cm during the consolidation phase. A variety of deformation rates are tested in this thesis, from a maximum rate of 25 cm/h to a slower rate like 0.005 cm/h.

3.3 Soil models

Plaxis provides the user with several material models simulating mechanical behaviour of soils and rocks. These models exhibit a various degree of accuracy, like Hooks law of linear, isotropic elasticity that only requires two input parameters (E and ν) to more advanced soil models with built-in features to account for soil behaviour such as memory of pre-consolidation, creep, swelling, strain-hardening/softening etc. In this thesis, the hardening soil model and a user-design model "Unified enhanced soft clay creep model" is used.

3.3.1 Hardening soil (HS)

HS model is an advanced model available in Plaxis, for simulating both stiff and soft soil behavior [24]. This model was originally proposed for sand, but later modified to be applicable for other types of soils. The basic feature of the HS model is that stiffness of the soil is stress dependent. Like the Mohr-Coulomb model, the limiting states of stress are described by the friction

angle (ϕ), cohesion (c) and the dilatancy angle (ψ). But in terms of soil stiffness, the HS model describes this with three different input parameters. These are triaxial stiffness (E_{50}), triaxial unloading stiffness (E_{ur}) and the oedometer loading stiffness (E_{oed}).

The HS model be considered as an advanced soil model, but there are some features that this model neglects. Softening due to soil dilatancy and debonding effects are not accounted for. Also, the model does not distinguish large stiffness at small strain levels and reduced stiffness at engineering strain levels [25].

Parameters	Value	Unit
γ_{unsat}	0	kN/m^3
γ_{sat}	0	kN/m^3
E_{50}^{ref}	2800	kPa
E_{oed}^{ref}	1100	kPa
E_{ur}^{ref}	28000	kPa
c_{ref}	0.5	kPa
ϕ	23	$^\circ$
ψ	-2	$^\circ$
ν	0.2	-
k_x, k_y	$6.5e^{-5}$	m/day
p_{ref}	100	kPa
Power(m)	1	-
K_0^{nc}	0.61	-

Table 3.1: Parameters for HS model.

The parameters used for the HS calculations are given in Table 3.1. These parameters are chosen to make the soil behave as a soft sensitive clay which is contracting while sheared.

3.3.2 Unified enhanced soft clay creep model (UESCC)

The UESCC model was created under the EU-CREEP project "Creep of geomaterials". This soil model is made with an extension to account for creep, and exhibits a rate dependent behaviour. The soil state is defined partly by the stress state, but also by 21 state variables and 21 equations providing constitutive behaviour. UESCC model requires 15 input parameters which is described in Table 3.2. Input parameters used for the calculations including unit weight, permeability and coefficient of lateral earth pressure are given in Table 3.3

Symbol	Units	Description
ϕ_{cs}	°	Internal critical state friction angle in triaxial compression
K_0^{NC}	-	Asymptotic value of horizontal stress over vertical stress in an oedometer condition
λ_i^*	-	Intrinsic volumetric compressibility parameter
r_{si}	-	The intrinsic creep number
X_0	-	Initial value of structure
ϕ_p	°	Mobilized internal friction angle at peak deviatoric stress
κ^*	-	Elastic volumetric compressibiity parameter
g^*	-	Elastic deviatoric compressibility parameter
a_v	-	Rate of destructuration
ω	-	Relative contribution to destructuration from plastic shear strains
OCR	-	Initial over-consolidation ratio
μ	-	The rate of rotation of reference and potential surfaces
β_{K0NC}	-	Initial rotation of reference surface
τ	day(s)	Reference time
OCR_{max}	-	Limit for creep induced OCR

Table 3.2: Parameters with description for UESCC model.

Parameters	Value	Unit
ϕ_{cs}	32	$^\circ$
K_0^{NC}	0.55	-
λ_i^*	0.06	-
r_{si}	500	-
X_0	9	-
ϕ_p	25	$^\circ$
κ^*	0.01	-
g^*	0.008	-
a_v	20	-
ω	0.3	-
OCR	1.6	-
μ	40	-
β_{K0NC}	0.25	-
τ	1	day(s)
OCR_{max}	1.7	-
k_x, k_y	$6.5e^{-5}$	m/day
γ	0	kN/m^3
K_0	0.55	-

Table 3.3: Parameters used for UESCC model.

Chapter 4

Results

Results from the calculations in plaxis for both soil models are presented in this chapter. Specifically, the results presented are failure modes, local drainage effects, excess pore pressure and torque with various rates.

4.1 Hardening soil model

4.1.1 Failure mode

Towards failure, the vane displays an expected circular failure mode which is triggered from the tip of each vane blade. At onset of rotation excess pore pressure is generated in front of the vane, leaving a slight field of suction behind each of the blades. By rotating the vane further, the excess pore pressure formation can be represented as a complete circle as presented in Figure 4.1, which is from a calculation with very fine mesh density (4186 elements) with a rate of 5 cm/h. From the principal strain evolution we can observe strain concentration towards failure. In FEM, the shear band appears more defined for faster rates.

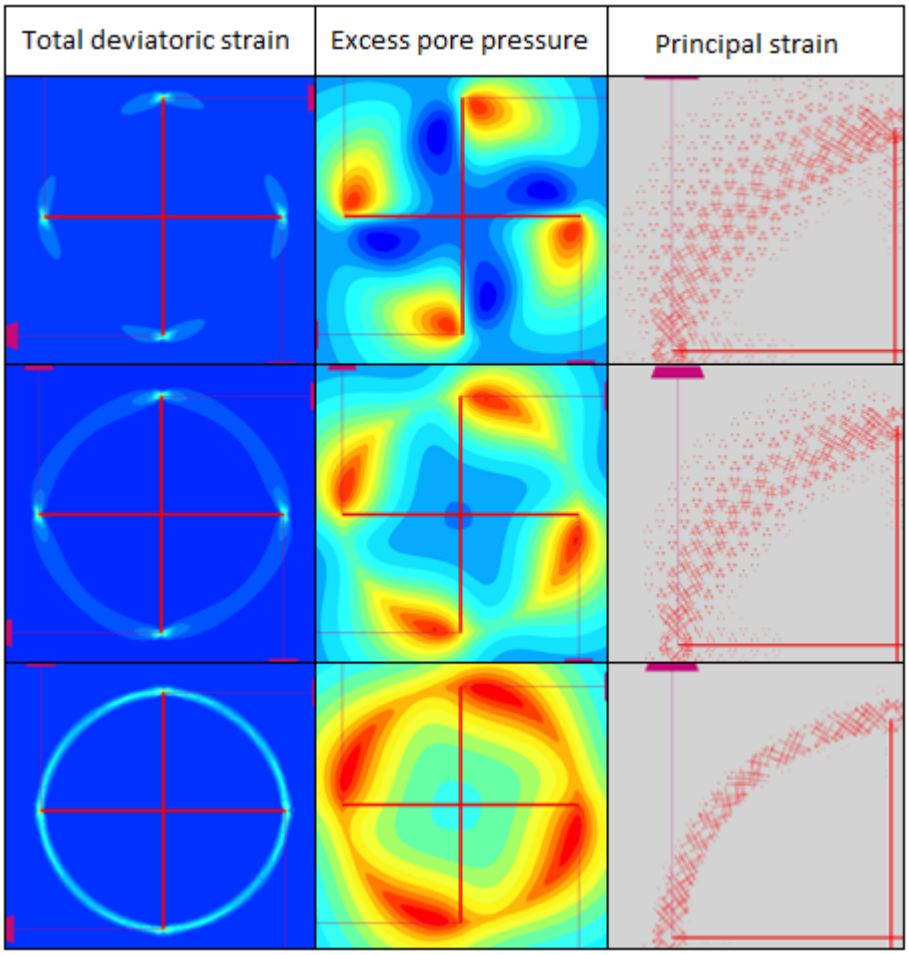

Figure 4.1: A step-wise presentation of total deviatoric strain, excess pore pressure and principal strain orientation towards failure for the vane modelled in Plaxis.

4.1.2 Local drainage and mesh density

Excess pore pressure distribution across a weak discontinuity can be represented by a Gaussian curve. The peak value increases as the vane progressively reaches the maximum yield state of the clay. Pore pressure evolution through 5 steps from a calculation with very fine element density (4186 elements) and a deformation rate of 5 cm/h can be seen all together in Figure 4.2 and step-wise with cross section locations in Figure 4.3. Stage 1 has a peak value of 51.8 kPa. However, the peak values barely changes as the rotation of the vane continues from stage 2 to 3 (50.3 and 49.5 kPa, respectively). Stage 4 shows a significant change in excess pore pressure as it is the highest overall peak value (62.9 kPa). Step 5 with a decreased peak-value of 53 kPa represents pore water dissipation, which also is illustrated by the shape of the curves as they become less concave for each step.

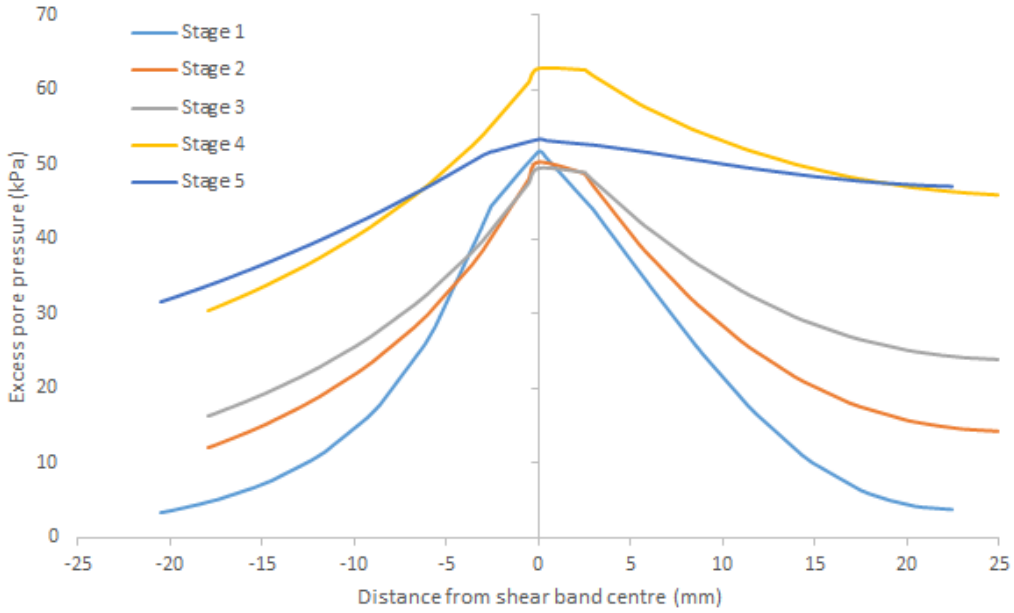

Figure 4.2: A 5 step excess pore pressure evolution across the shear band

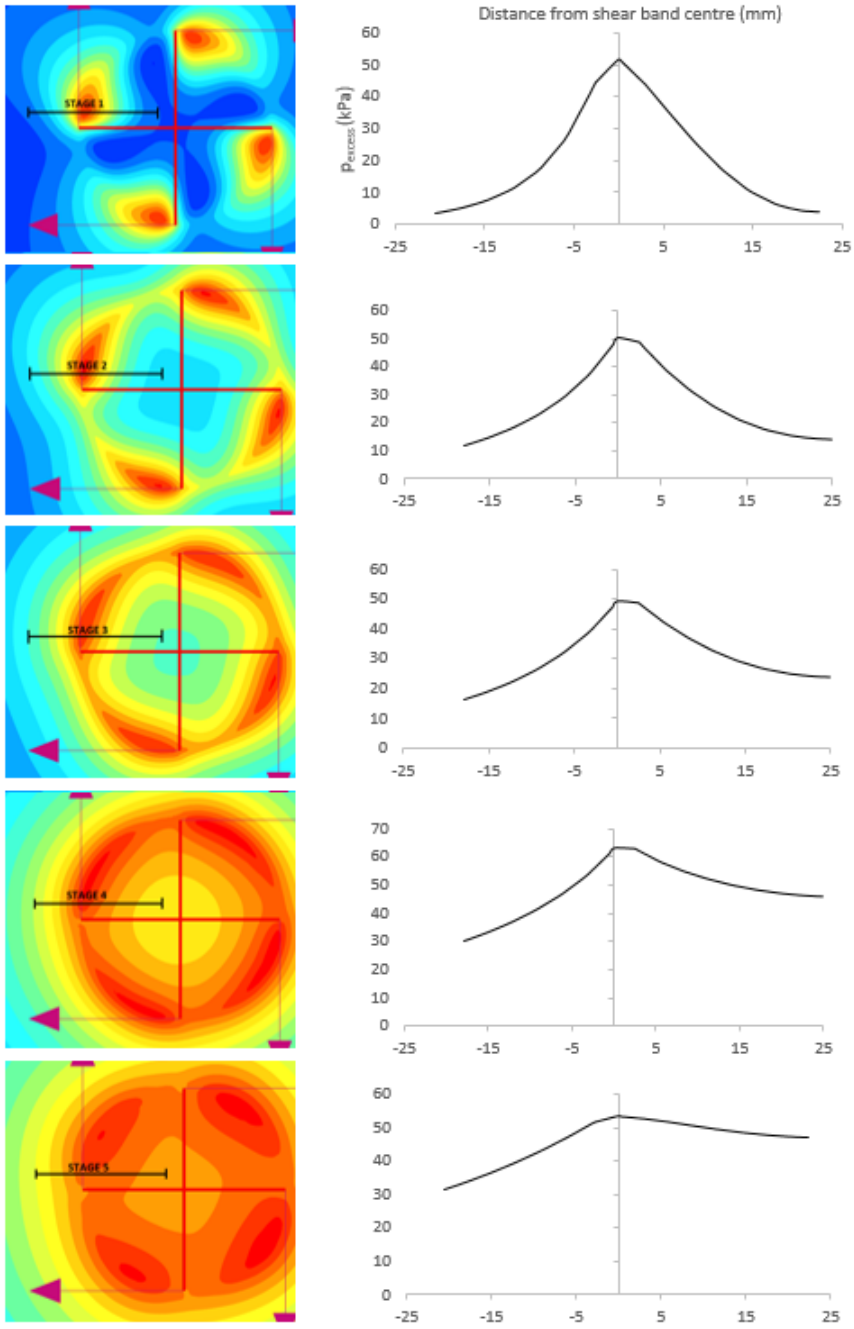

Figure 4.3: Evolution of excess pore pressure for a rate of 5 cm/h with HS.

By using the same coordinates in Plaxis to draw cross sections for several mesh densities it was observed that the mesh design became a sensitive factor for the local drainage from the shear band. Results from coarse, medium and fine mesh can be seen in Appendix A.1. The coarse and medium refined mesh gave an asymmetrical pore pressure build up where a distinctive field of pore pressure concentration could be observed under the right vane blade. Curves also became less smooth, due to less defined discretization.

Mesh quality	Peak-values (kPa)
Coarse	51.4
Medium	57
Fine	55.8
Very fine	62.9

Table 4.1: Peak-values for all meshes

4.1.3 Excess pore pressure with various rates

By using cross section view in Plaxis, a graphical representation of excess pore pressure for different rates can be seen in Figure 4.4. Location of the cross section is the same as in Section 4.1.2, but these results are taken from the same time-step for various rates. A high excess pore pressure generation of 89.1 kPa is initiated by the fastest rate of 25 cm/h, which is expected for narrow shear band formations at higher rates. Peak-values are gradually reducing with slower rates. The slowest rate tested is 0.125 cm/h, which ended up with a peak-value of 11.2 kPa. The apparent rate-dependant pore pressure generation was also calculated with other mesh densities. A comparison of excess pore pressure across the shear band for various mesh densities are presented in Figure 4.5, which yet again demonstrates mesh dependency as the peak-values differs with 34 % at the most. Highest peak-value is observed from the coarse mesh with 64.3 kPa and lowest from fine mesh with 45.5 kPa. Peak-values for very fine and medium mesh density is 50.3 and 56.6 kPa, respectively. A more comprehensive presentation of the results for all meshes can be found in Appendix A.1.2.

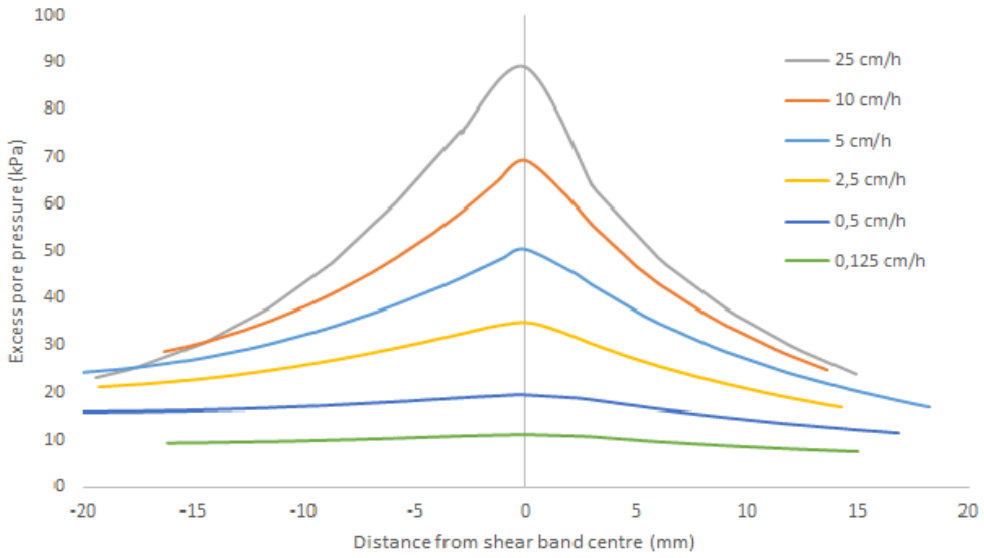

Figure 4.4: Excess pore pressure presentation with 4186 elements.

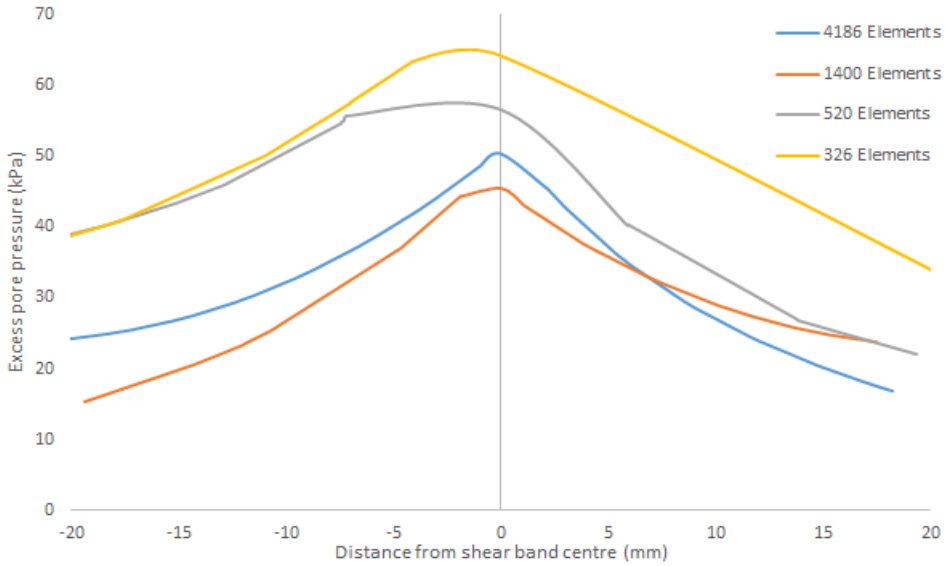

Figure 4.5: Excess pore pressure comparison for various mesh densities for a rate of 5 cm/h.

4.1.4 Torque with various rates

Maximum torque for various rates are analyzed from a point located at the top of the vane blade, indicated by the yellow circle in Figure 4.6(a). Outputs are expected to be symmetrical. A control was done to ensure that maximum torque for top and bottom blade indicated equilibrium, which can be seen from Figure 4.6(b) for a simulation with 5 cm/h.

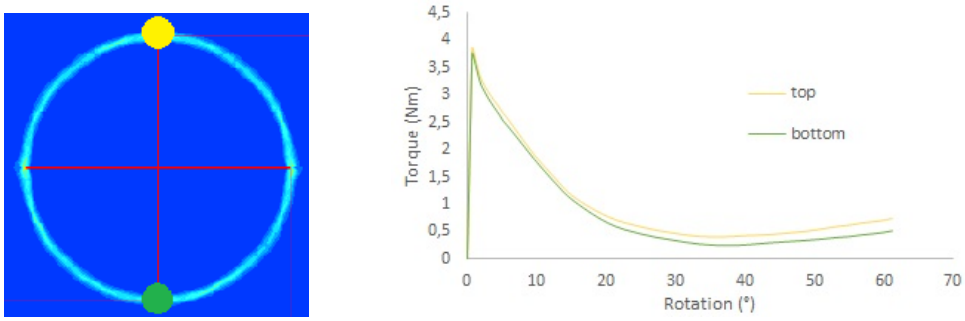

(a) Points of interests

(b) Torque/rotation relation

Figure 4.6: The vanes behaviour for top and bottom point upon deformation.

Several rates of deformation have been prescribed to the vane, resulting in various torque-rotation relations upon further rotation after peak-strength. Every rate has its own singular softening response, where the decrease in strength are more dramatic for higher deformation rates. Figure 4.7 displays the results for all rates with a very fine mesh of 4186 elements. Results with different mesh qualities can be seen in Appendix B.1. Failure is observed at peak-values, which is around 1° rotation for all rates. Peak-strength values for faster rates are around 3.8 Nm, but as the rates decreases, a higher peak-strength can be observed. Maximum peak-strength is 4.2 Nm, which is for a slow rate of $2.08e^{-5}$ cm/h. Briefly summarized, peak-strength is more or less constant for all rates, but peak-strength increases as the rates become very low. Faster rates after peak-values exhibits a relatively higher decrease than slower rates.

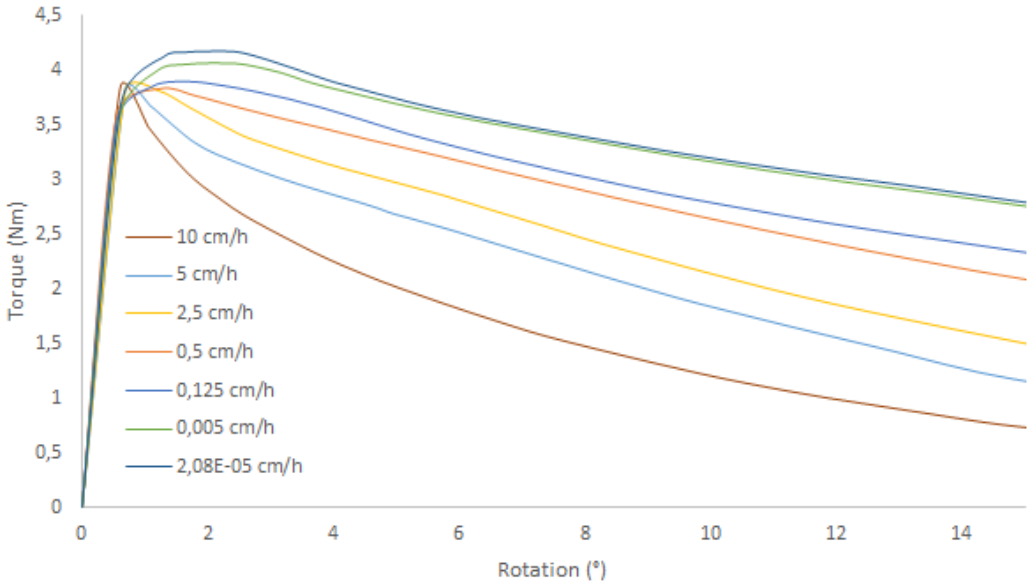

Figure 4.7: Torque/rotation relation for vane modelled in FEM.

It is of interested to obtain mesh dependant results. Figure 4.8 highlights the change of shear band thickness with plastic points due to different mesh refinements when deformation rate is kept constant. Comparisons of results from rates of 0.5 cm/h and 10 cm/h with all mesh refinements are given in Figure 4.9 and 4.10. It can be seen that the HS model certainly generates non-unique answers. Both graphs indicates that improved mesh qualities results in higher peak-values, ranging from 3.8 Nm at highest to 3.2 Nm.

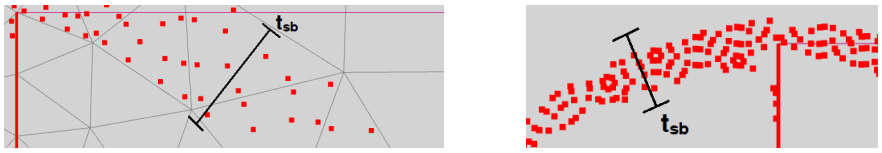

(a) Coarse, t_{sb}=4mm (b) Very fine, t_{sb}=2mm

Figure 4.8: Measured shear band thickness for a rate of 10 cm/h for different mesh qualities: (**a**) Coarshe mesh, (**b**) Very fine mesh.

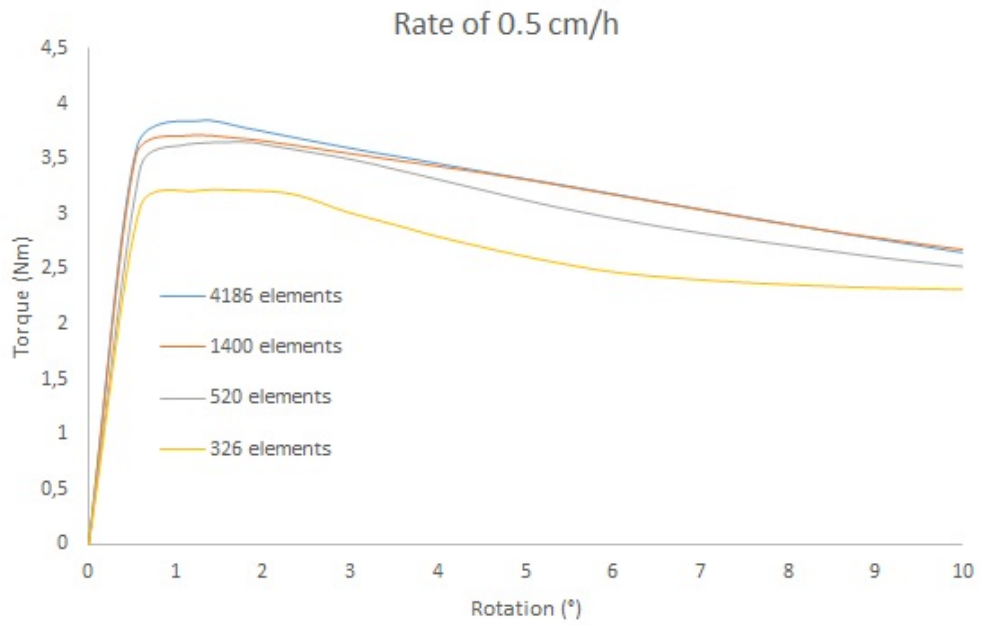

Figure 4.9: Mesh comparison for a rate of 0.5 cm/h.

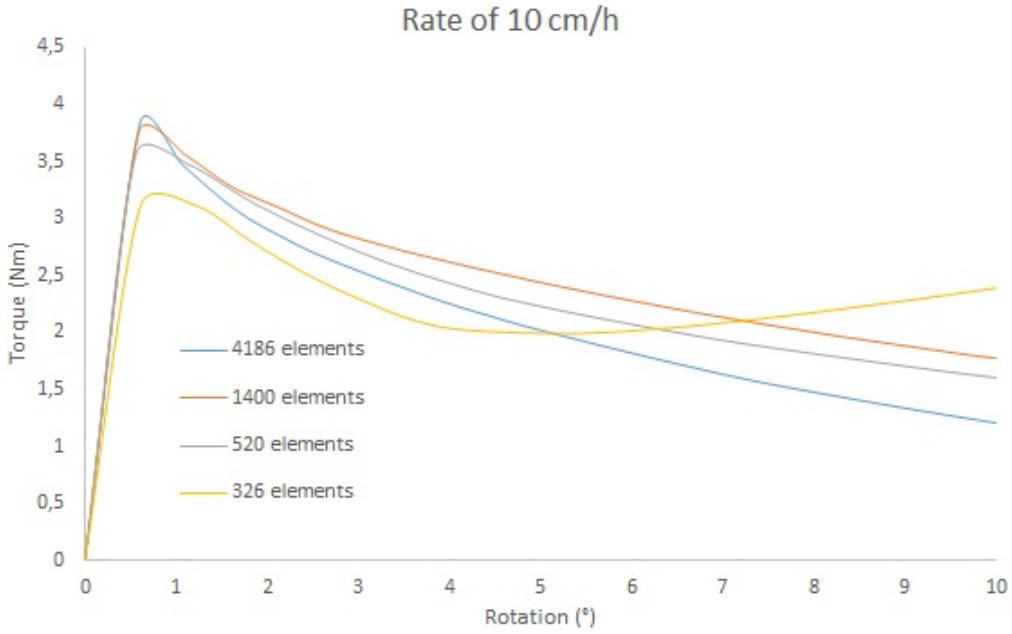

Figure 4.10: Mesh comparison for a rate of 10 cm/h.

4.2 Unified enhanced soft clay creep model

4.2.1 Failure mode

For UESCC model calculations, a field of very high suction can be seen from behind the blades as the rotation progresses. These maximum stress locations are indicated as red in Figure 4.12. A very high suction of 160 kPa is constant through all 3 stages and excess pore pressure increases from 30 to 80 kPa. Excess pore pressure does not encircle the vane as could be seen from calculations with hardening soil model. The distinctive stress zones of suction are kept in the same location for all steps towards failure. A failure mode in terms of state parameter x can be seen from Figure 4.11. The dimensionless scale from 1 to 10 indicates the remoulded state, where 1 is completely remoulded and 10 is undisturbed. This failure mode is in resemblance to the experimentally observed failure mode discussed in Section 2.2.

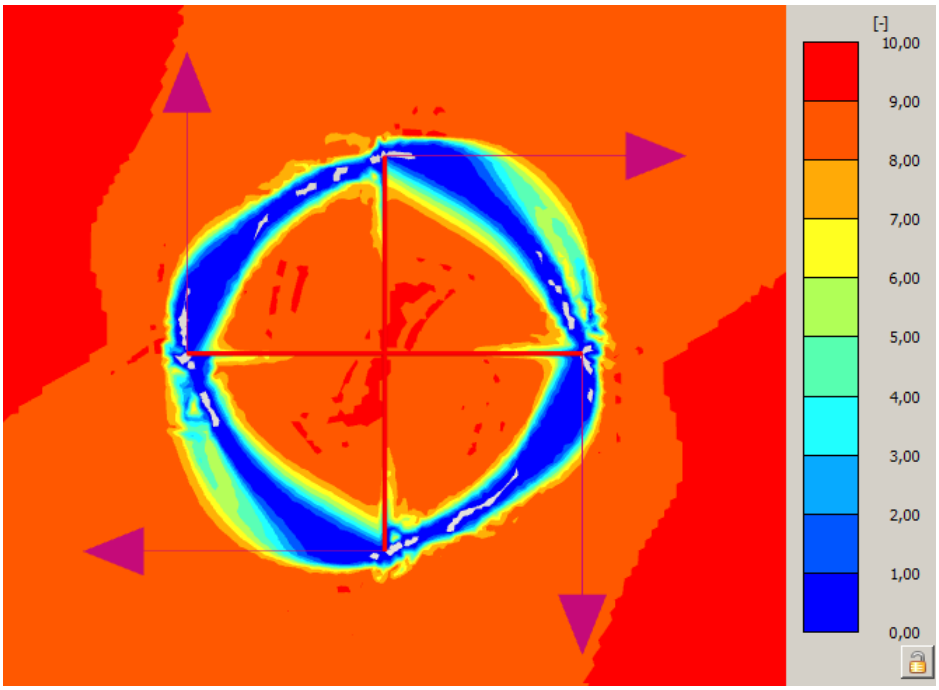

Figure 4.11: Plaxis output of state parameter x with UESCC model.

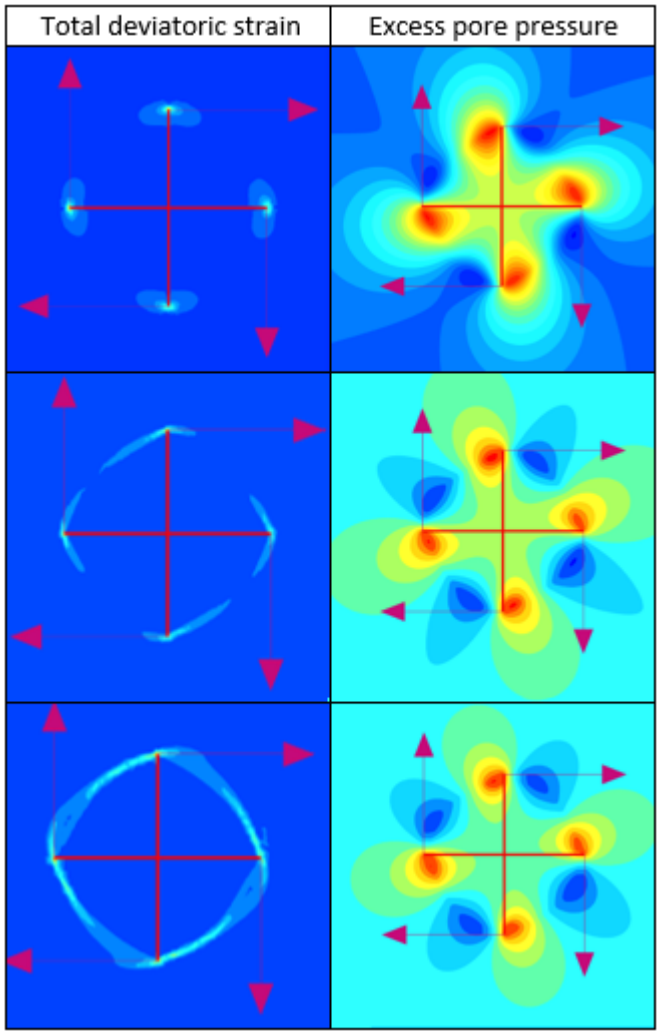

Figure 4.12: A step-wise presentation of total deviatoric strain and excess pore pressure towards failure.

4.2.2 Local drainage and mesh density

Like for the HS model, step-wise results were obtained to understand the draining effects. Figure 4.13 demonstrates the excess pore pressure evolution for a rate of 5 cm/h and very fine mesh quality. A step-wise illustration of the pore pressure generation is given in Figure 4.14. Pore pressure builds up until peak value of 57.3 kPa in stage 3, then reduces as pore pressure dissipate to the last registered value of 53.7 kPa. Based on the pore pressure evolution presented, the dominant presence of suction affects results obtained from the cross section drawn across the shear band. Suction is presented as negative values 5-15 mm from the shear band centre towards the exterior soil body. Another conspicuous thing about these results is the consistent location of the stress fields, which acts independent from step to step towards failure.

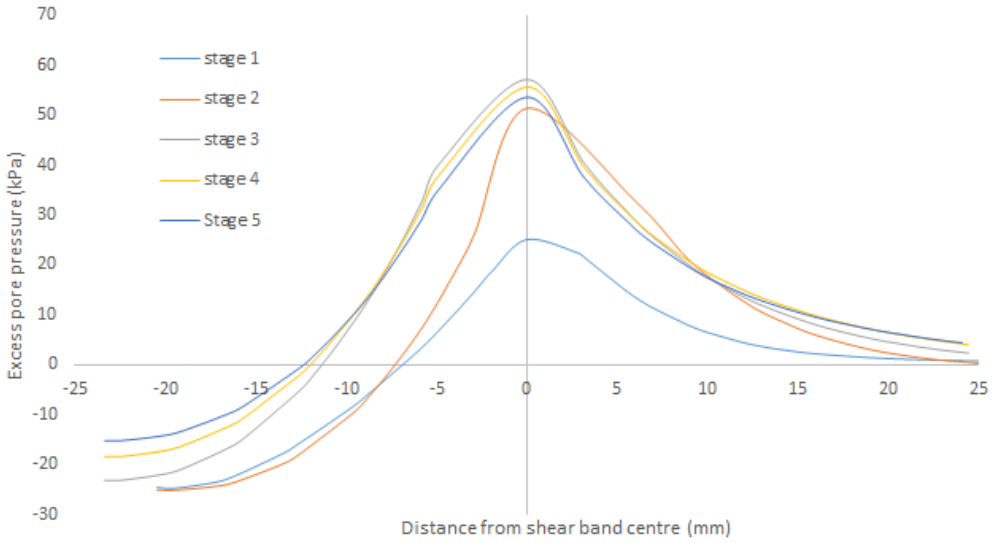

Figure 4.13: A 5 step excess pore pressure evolution across the shear band with UESCC model

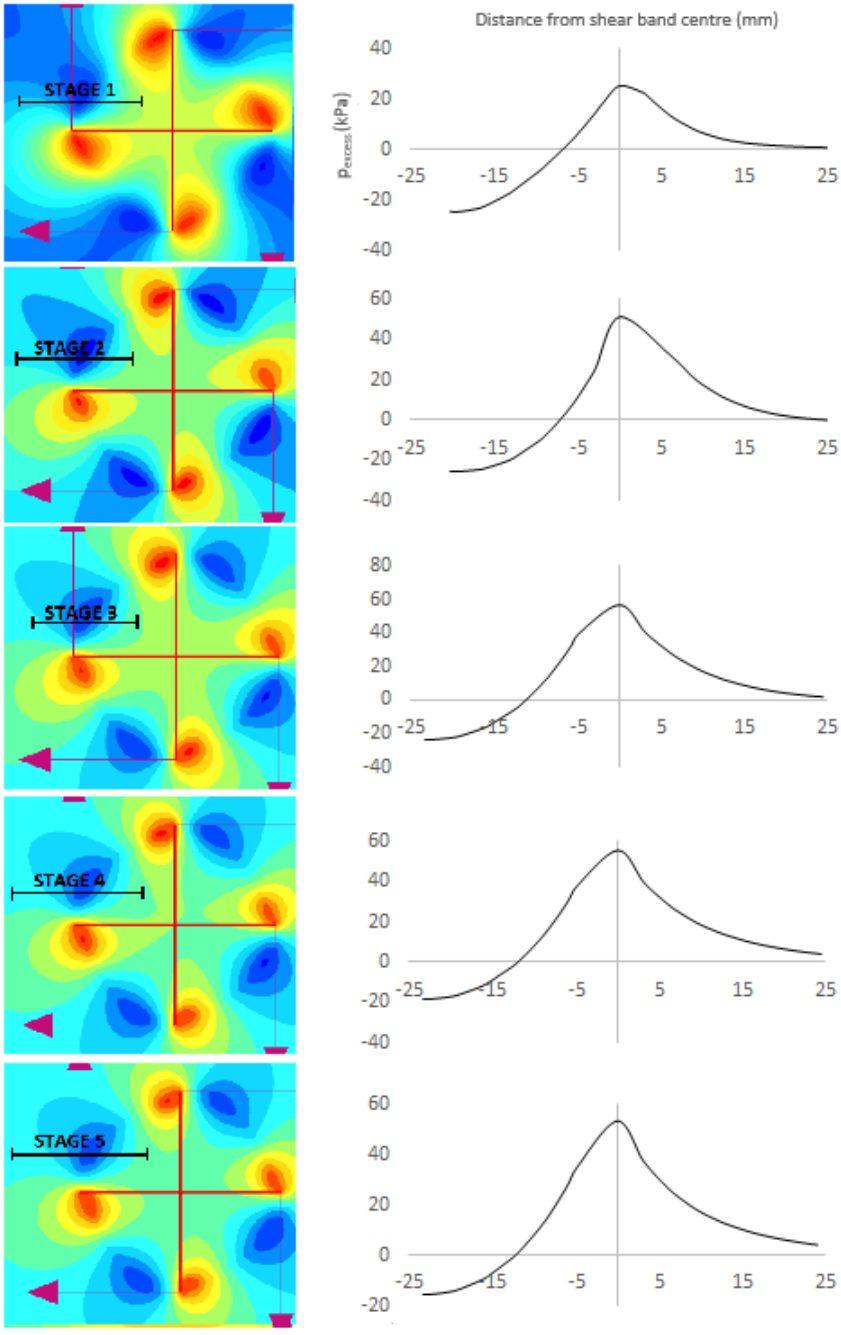

Figure 4.14: Evolution of excess pore pressure for a rate of 5 cm/h with UESCC model.

Results for fine, medium and coarse mesh density can be found in Appendix A.2.1. Every mesh generates results with suction near the shear band centre.

4.2.3 Excess pore pressure with various rates

Excess pore pressure distributions over a consistent cross section location for UESCC model are given in Figure 4.15. Results are presented for 5 rates from 25 to 0.5 cm/h and displays that higher rates will generate more concentrated pressure and higher peak-values at the shear band centre. Highest peak value is 101.5 kPa for 25 cm/h, and at lowest 8.8 kPa for 0.5 cm/h. A comparison for the same time-step of excess pore pressure distribution along the shear band for all mesh refinements are given in Figure 4.16. The comparison shows that the coarse mesh has the highest peak-value, but the other mesh qualities are relatively close. Results for all rates with fine, medium and coarse mesh are presented in Appendix A.2.2

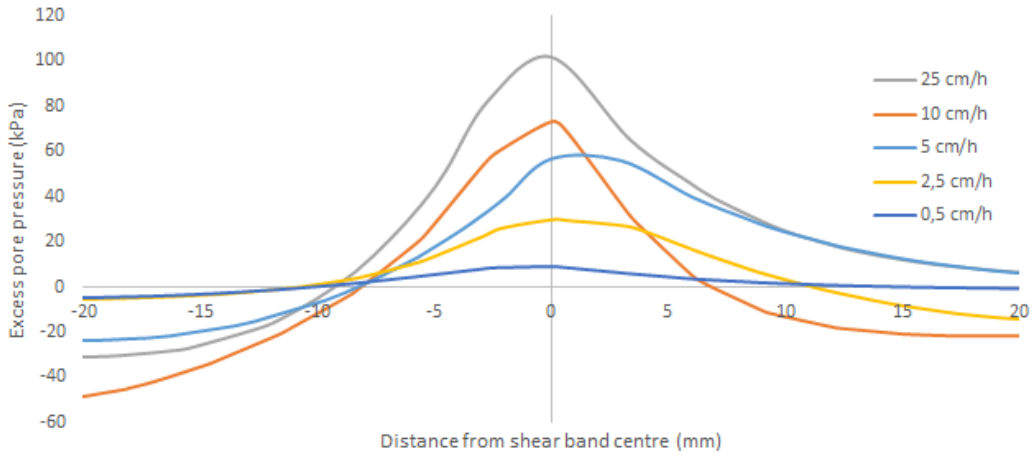

Figure 4.15: Excess pore pressure presentation for UESCC with 4186 elements.

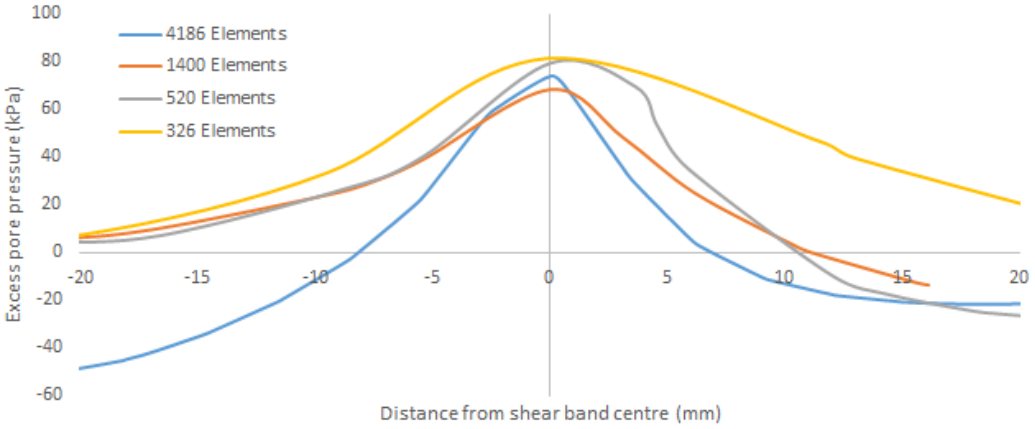

Figure 4.16: Mesh comparison of excess pore pressure for a rate of 10 cm/h.

4.2.4 Torque with various rates

Results for maximum torque for various rates are gathered with a similar approach as for the Hardening soil model(Section 4.1.4). Figure 4.17 describes the torque strength towards and after failure. Failure is observed at an early stage of around 0.5-1° for all rates. The residual state of the clay are clearly indicated as the curves flattens at higher rotation. Contrary to results for HS, these curves are acting rate-dependently. Higher rates results in higher peak-values, but also exhibits a steeper decrease towards a lower residual strength. Calculations for all rates were stopped at different stages after failure due to "run time error in kernel" or "NaN found during calculation" which can be seen from the results. The highest peak-value is 10.7 Nm for 10 cm/h and lowest is 8.7 Nm for 0.05 cm/h, which appears to be drained. Torque strengths for various rates with fine, medium and coarse mesh can be seen in Appendix B.2. A comparison of the torque/rotation relation for all meshes are given in Figure 4.19 for a rate of 10 cm/h and Figure 4.18 for 0.5 cm/h. It can be seen from mesh comparisons that all curves are singular, but not completely different. Results from the slower rate of 0.5 cm/h, displays larger similarities than for 10 cm/h. For faster rates, the different results from the meshes separates after peak.

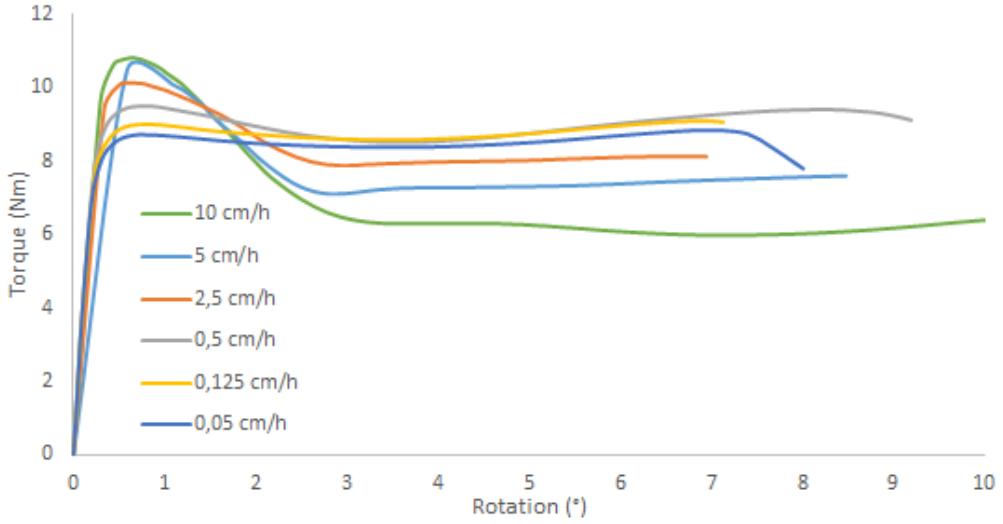

Figure 4.17: Torque-rotation relation for vane modelled in FEM with UESCC.

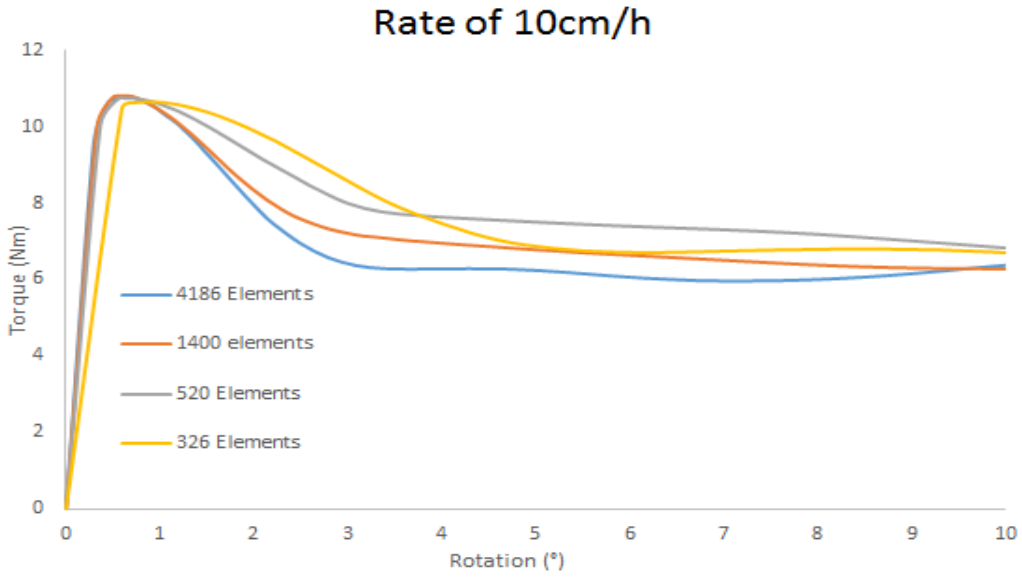

Figure 4.18: Mesh comparison for a rate of 10 cm/h with UESCC.

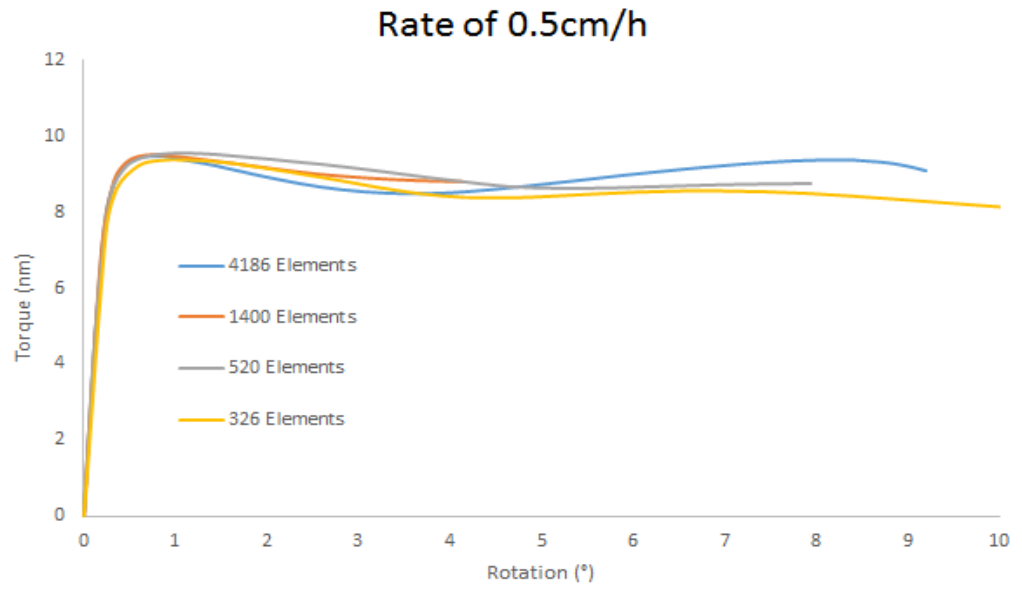

Figure 4.19: Mesh comparison for a rate of 0.5 cm/h with UESCC.

Chapter 5

Discussion and Conclusion

5.1 Discussion

Results of strain-softening material behaviour for a soft clay is achieved in this FEM analysis for a modelled shear vane investigation. Mesh density has proven to be a decisive factor, as results have been compared between 4 consistent mesh refinements for all cases. Numerically observed shear band formations and step-wise draining effects have been elaborated for HS and UESSC. Maximum torque-strength and excess pore pressure build-up have been investigated with several deformation rates.

Results for HS displayed a perfect circular shear band formation with excess pore pressure build-up in front of each vane blade. By rotating the modelled vane further, excess pore pressure encircled the vane. Excess pore pressure evolution is observed by prescribed cross sections across emerged shear bands for 5 steps towards failure. Pore pressure distribution from HS can be represented by a Gaussian curve that gradually becomes more horizontal as pore pressure dissipates post-failure. HS displayed higher excess pore pressures across the shear band centre for higher deformation rates (Figure 4.4). Torque-strength showed higher peak-strengths for very slow rates (Figure 4.7), which can be explained by the small amount of pore pressure generation. From the results and discussion about strain-softening charac-

teristics in Section 2.1.2, it can be assumed that HS is not rate-dependant. Comparisons of all mesh refinements also indicated mesh dependency since there could not be observed any distinctive uniqueness.

As HS proved insufficient, a rate-dependent model was used. UESCC simulations showed failure modes that were shaped more like a well-rounded square (Figure 4.11), which may be more realistic as it has been experimentally observed (Figure 2.7). By investigating pore pressure evolution around the vane, it could be seen that zones with concentrated excess pore pressure were located in front of each vane blade for all steps. Unlike HS simulations, excess pore pressure never completed the circular pattern towards or post-failure. Suction became a very dominant component in the Plaxis 2D outputs for UESSC calculations. Suction behind the vane blades is expected in this case, but not of maximum values of 60-80 kPa. It seems that UESSC responds like there is no tension cut-off criterion. In terms of pore pressure generation across the shear band with different rates, UESSC resulted in similar characteristics as for HS. Faster rates develops higher peak-values. Results considering Torque-strengths for various rates clearly displayed rate-dependency (Figure 4.17). Faster rates resulted in higher peak-values with even steeper softening response. Mesh comparisons were done with UESCC, which resulted in non-unique answers. The comparison for 10 cm/h (Figure 4.19) displays similarities for finer mesh refinements, but separates at the residual phase. Mesh comparison for a slow rate of 0.5 cm/h (Figure 4.18) shows some interesting results as all mesh refinements are relatively close, but not unique.

5.2 Conclusion

In this study, the effects of mesh refinement has proven to be sensitive for Plaxis 2D outputs in the framework of strain-softening and local drainage mechanics for a soft clay. Results from HS model appeared rate-independent. Calculations with UESSC model generated results which followed the strain-softening characteristics elaborated in Section 2.1.2. Results from UESSC became less diverse than HS when compared with all mesh refinements, but mesh dependant results could not be achieved.

Bibliography

[1] Aas G. Gregersen O. Karlsrud, K. Can we predict landslide hazards in soft sensitive clays? summary of norwegian practice and experiences. *in 'Proc. 4th Int. Symp. Landslides, Toronto'*, 1:107–130, 1984.

[2] K. Terzaghi. Ends and means in soil mechanics. *Eng. Journ. (Canada). 27 : 608*, 1944.

[3] Statens Vegvesen. Laboratorieundersøkelser. *Håndbok 014*, Vedlegg 1:4, 2005.

[4] Steinar Nordal. Geotechnical engineering, advanced course. *NTNU, Compendium*, page Chapter 6, 2017.

[5] Hicher P. Hattab M. Dilating behaviour of over consolidated clay. *Soils and foundations*, 44(4):27–40, 2004.

[6] L. Berre, T. Bjerrum. Shear strength of normally consolidated clays. *Proc. 8th Int. Conf. Soil Mech. Found. Eng., Moscow, Vol 1*, pages 39–49, 1973.

[7] K. Lunne, T. Andersen. Soft clay shear strength parameters for deep-water geotechnical design. *Proc. 6th Int. Conf. Offshore Site Investig. and Geotech., London*, pages 151–176, 2007.

[8] Svensk I. Bernander S. On the brittleness of clays. *Symposium on soft clays*, pages 99–112, 1982.

[9] Holmberg G. Bernander J. Isacsson K. Bernander S., Svensk I. Shear strength deformation properties of clays in direct shear tests at high

strain rates. *Proceedings of the 11th international conference soil mechanics foundation engineering*, pages 987–990, 1985.

[10] Thakur V. Jostad HP., Andresen L. Calculation of shear band thickness in sensitive clays. *Proceedings of the 6th European conference numerical methods in geotechnical engineering, Graz*, pages 27–32, 2006.

[11] V. Thakur. Numerically observed shear bands in soft sensitive clay. *Geomech Geoeng 6(2)*, pages 131–146, 2011.

[12] Anders Gylland. Material and slope failure in sensitive clays. 2012.

[13] Bernander S. Long-term stability of clay slopes. *Géotechnique*, 14(2):75–102, 1964.

[14] Georgiannou VN et al. Burland JB, Rampello S. A laboratory study of the strength of four stiff clays. *Géotechnique*, 47(3):491–514, 1997.

[15] Septanika EG et al. Vermeer PA, Vogler U. Modelling strong discontinuities in geotechnical problems. *Proceedings of the 2nd international symposium on continuous and discontinuous modelling of Cohesive Frictional Materials*, CDM 2004:381–394, 2004.

[16] Janbu N. Soil models in offshore engineering. *Géotechnique*, 35(3):241–281, 1985.

[17] Bernander S. Progressive landslides in long natural slopes. *Licentiate thesis, Luleå*, 2000.

[18] Contreas I.A. Stark T.D. Constant volume ring shear apparatus. *GTJ*, 19(1):3–11, 1996.

[19] K.H. Roscoe. The influence of strains in soil mechanics. *Geotechnique*, 20:129–170, 1970.

[20] V. Thakur. Strain localization in ss clays. thesis (phd). *The Norwegian University of Science and Technology*, 2007.

[21] Vegdirektoratet Statens Vegvesen. Felundersøkelser. *Håndbok R211*, page 29, 2014.

[22] Z. Bazant. Instability, ductility and size effects in strain-softening concrete. *Journal of the Engineering Mechanics Division, ASCE 102(2)*, pages 331–344, 1976.

[23] Z. Pietruszczak, S. Mròz. Finite element analysis of deformation of strain-softening materials. *International Journal for Numerical Methods in Engineering 17*, pages 327–334, 1981.

[24] T. Schanz. The hardening soil model: Formulation and verification. *Beyond 2000 in computional Geotechnics - 10 years of PLAXIS*, 1998.

[25] Plaxis. Material models manual. pages 69–82, 2018.

Appendix A

Local drainage

This appendix contains further results from FEM regarding excess pore pressure development with coarse, medium and fine mesh quality for HS and UESSC soil model.

A.1 Hardening soil model

As a supplement to the analysis in Section 4.1.2 and Section 4.1.3, a step-wise calculation for coarse, medium and fine mesh quality has been done with HS model. This appendix also provides results for excess pore pressure across the shear band with various rates.

A.1.1 Excess pore pressure evolution

The results represented from Figure A.1, A.2 and A.3, displays the variations of peak-values and pore pressure dissipation due to different mesh refinements in Plaxis for a deformation rate of 5 cm/h. It can be observed that curves for higher mesh densities is smoother due to improved discretization in FEM.

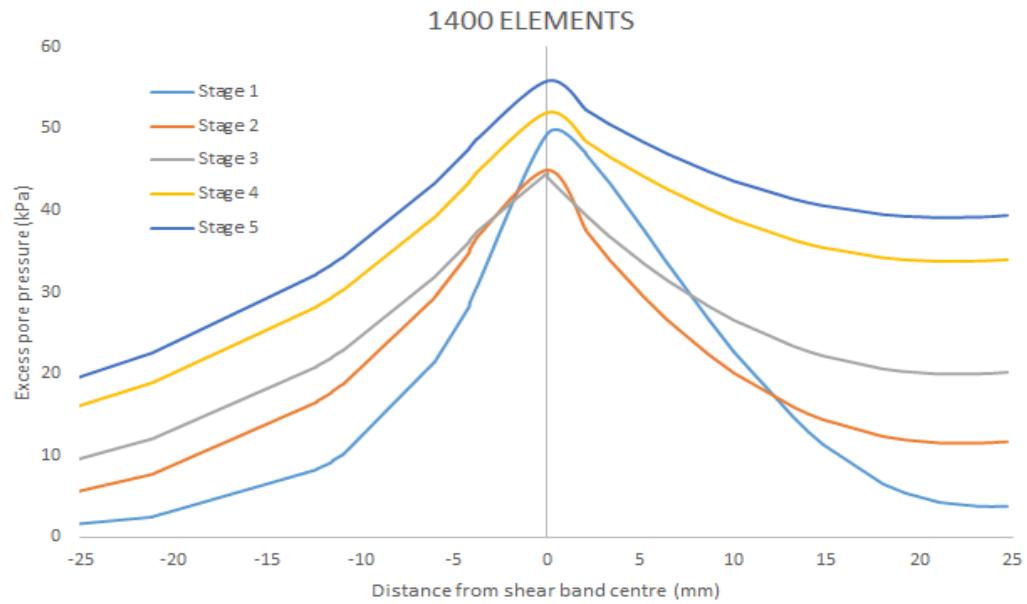

Figure A.1: Excess pore pressure presentation with 1400 elements.

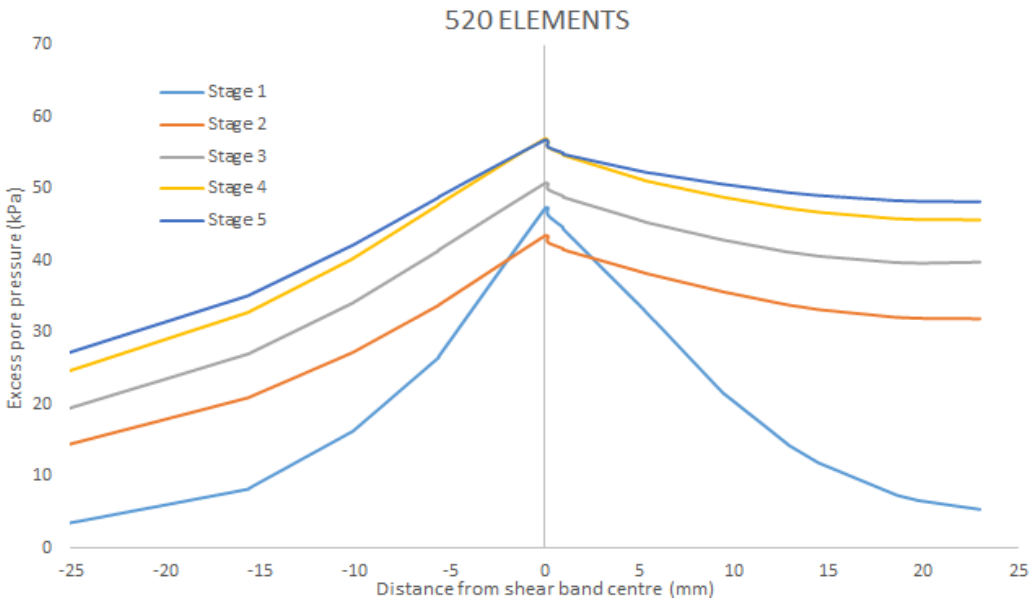

Figure A.2: Excess pore pressure presentation with 520 elements.

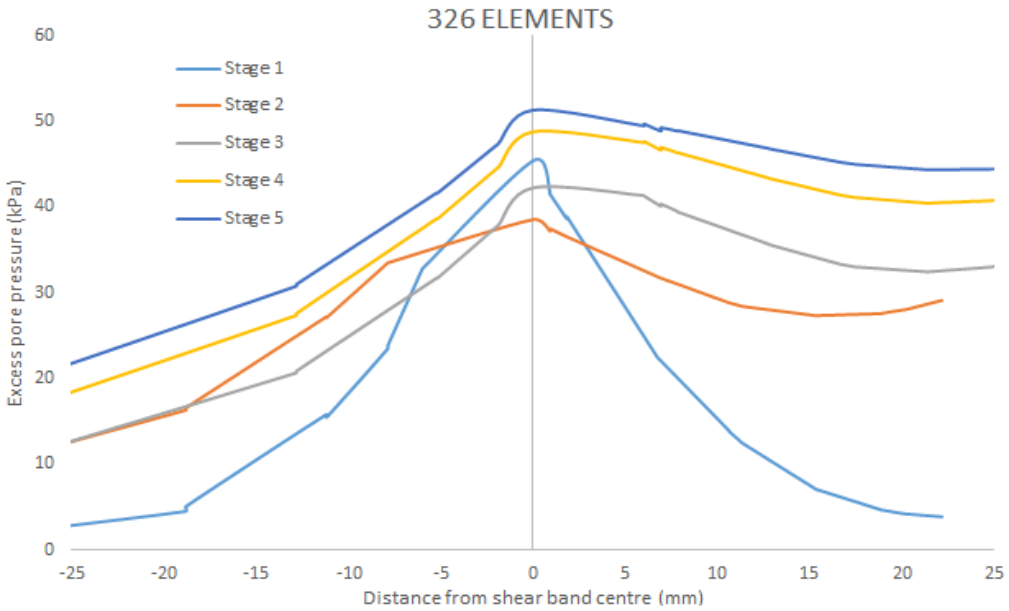

Figure A.3: Excess pore pressure presentation with 520 elements.

A step-wise screenshot collage can be seen in Figure A.4. By inflicting the vane a rotation, excess pore pressure gradually encircles around the vane. However, mesh refinement is a decisive factor for the results. Mesh qualities of 326 and 520 elements gave results indicating an asymmetrical excess pore pressure development. A distinct field of excess pore pressure build up located under the right vane blade can be seen from simulations with mesh densities of 326 and 520 elements. The simulation is modelled for the excess pore pressure to emerge symmetrical upon deformation, which can be seen from the 1400 element simulation.

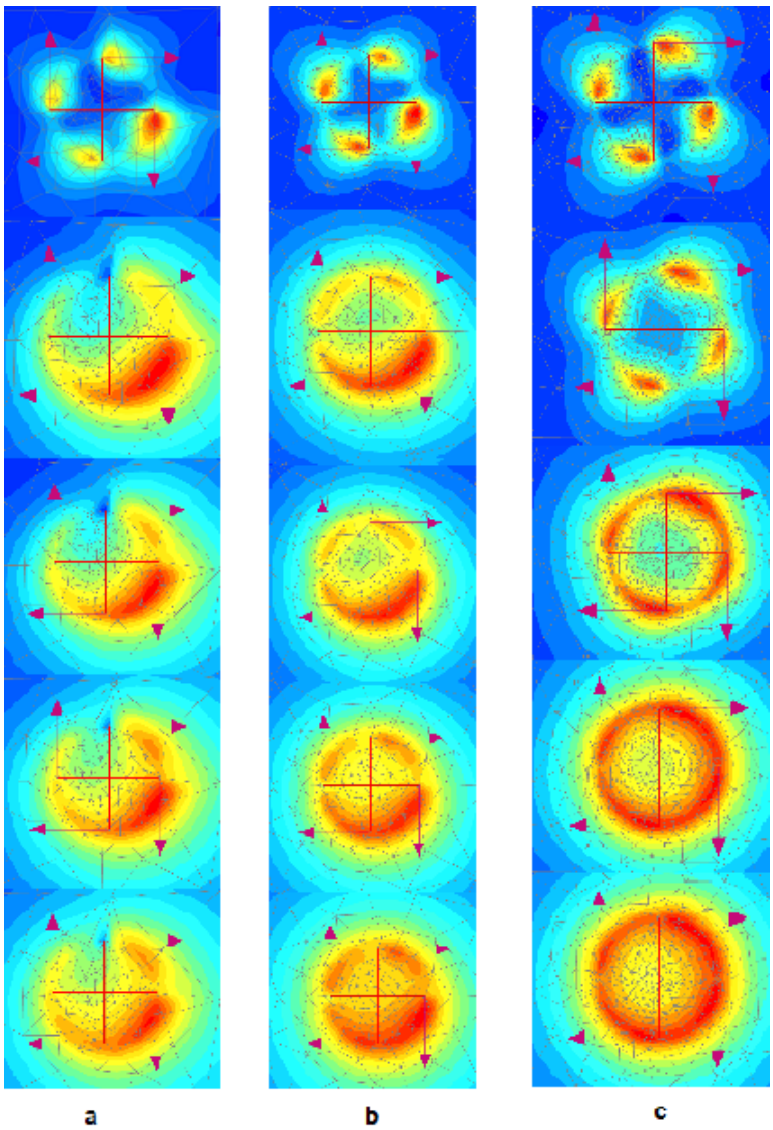

Figure A.4: Excess pore pressure through 5 steps with (**a**) 326 elements, (**b**) 520 elements and (**c**) 1400 elements.

A.1.2 Various rates and mesh densities

Results with fine, medium and coarse mesh refinement are presented in Figure A.5, A.6 and A.7. All the figures demonstrates a pore pressure generation tendency where higher rates results in higher peak-values in the centre of the shear band. Another notable observation is that lower mesh qualities in this case displays a skewness which can in addition to discretization also be a consequence of the circular failure mode. All meshes displays peak-values that are correctly in order relative to each other, but varies significantly if the same rate is compared between meshes. Interestingly, coarse and medium mesh refinement displays a much higher difference in peak-value for faster rates compared to the fine mesh.

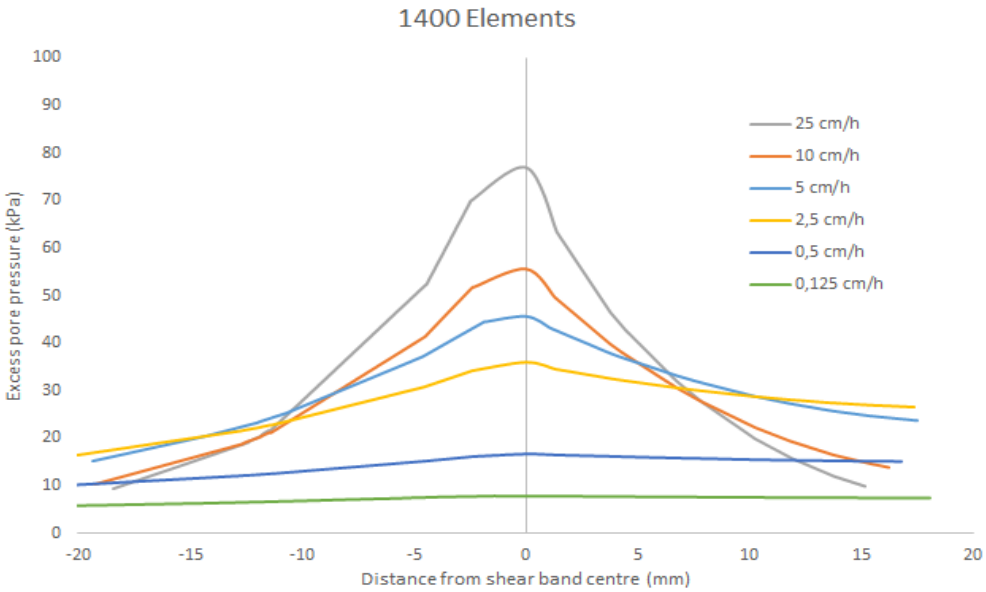

Figure A.5: Excess pore pressure distribution for the same time-step with various rates and 1400 element mesh refinement.

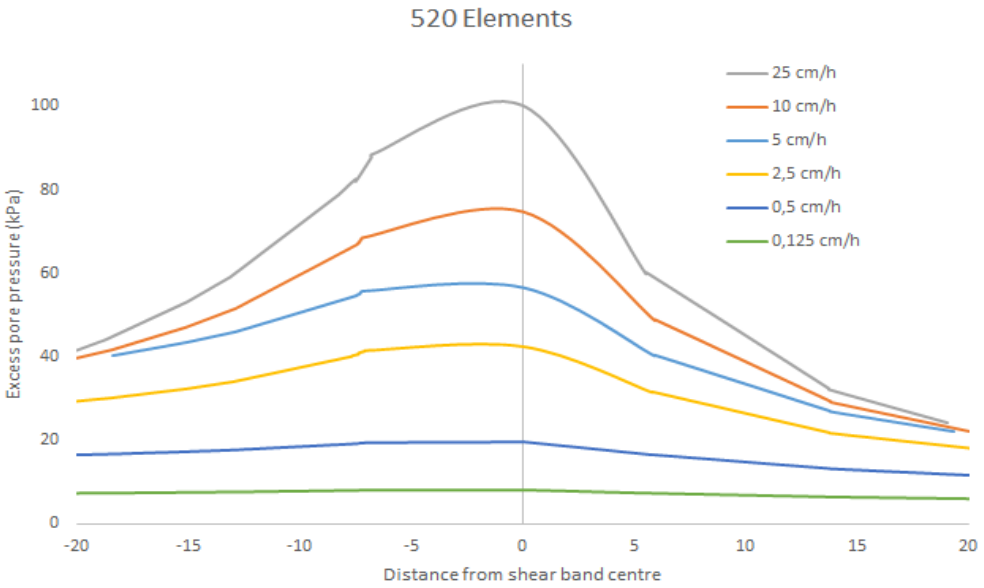

Figure A.6: Excess pore pressure distribution for the same time-step with various rates and 520 element mesh refinement.

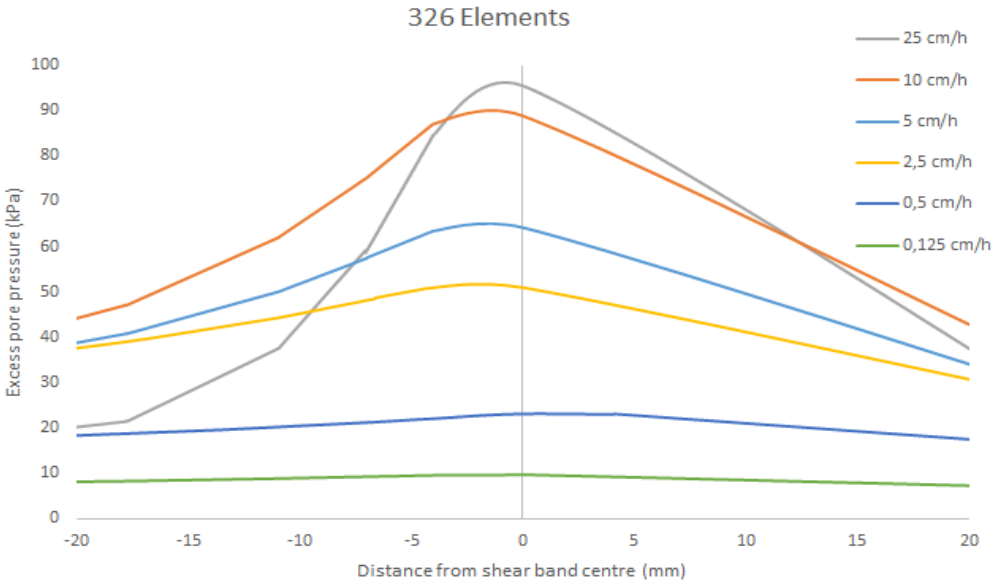

Figure A.7: Excess pore pressure distribution for the same time-step with various rates and 326 element mesh refinement.

A.2 Unified enhanced soft clay creep model

As a supplement to the analysis in Section 4.2.2 and Section 4.2.3, a stepwise calculation for coarse, medium and fine mesh quality has been done with UESSC model. This appendix also provides results for excess pore pressure across the shear band with various rates.

A.2.1 Excess pore pressure evolution

Results from fine, medium and coarse mesh densities are presented in Figure A.8, A.9 and A.10 below for a deformation rate of 5 cm/h. It can be seen that suction affects the results as they all are becoming negative at higher distances from the shear band centre.

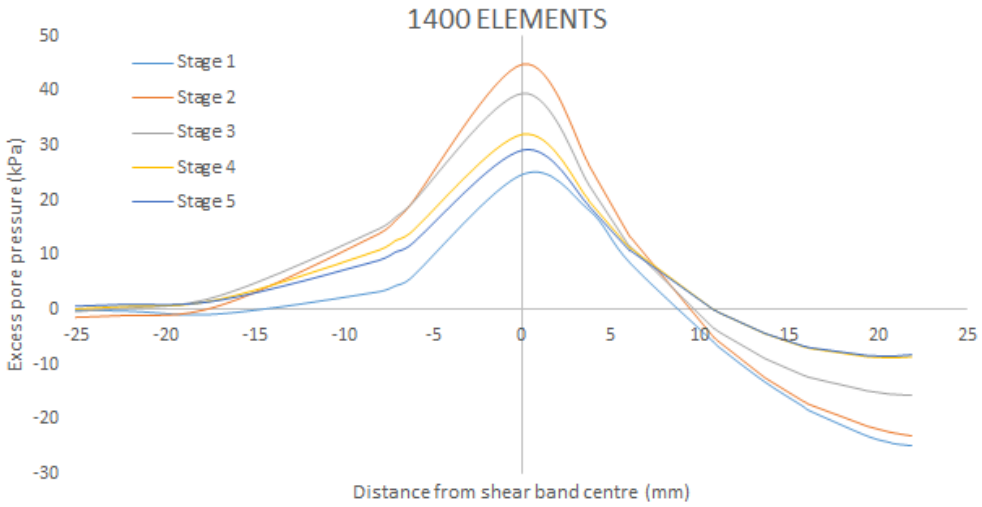

Figure A.8: Excess pore pressure presentation for UESCC with 1400 elements.

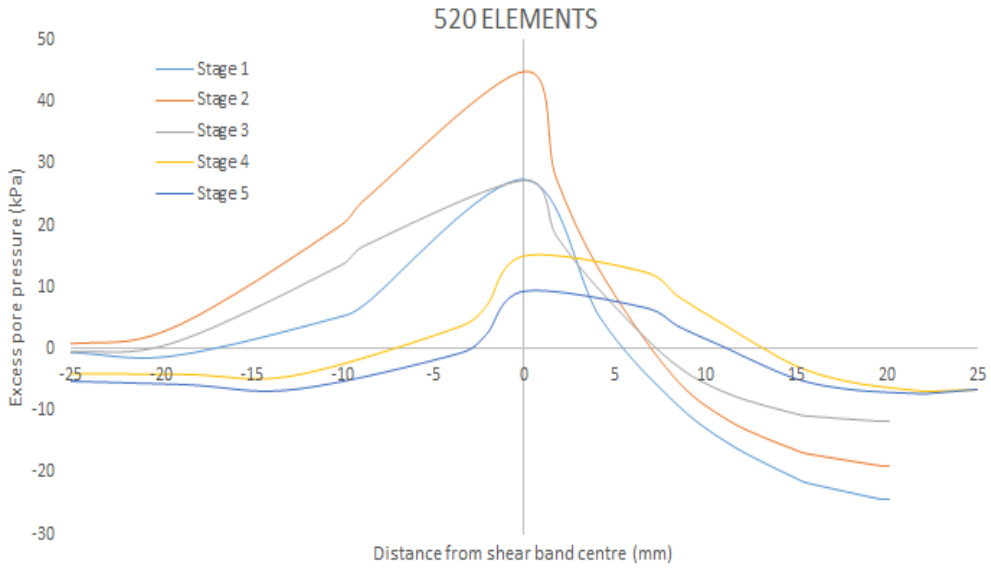

Figure A.9: Excess pore pressure presentation for UESCC with 520 elements

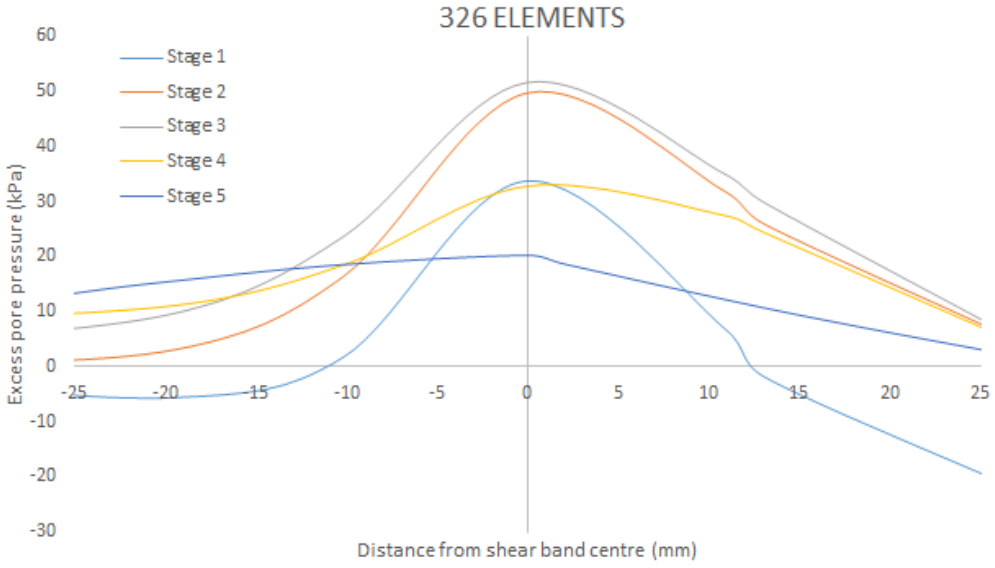

Figure A.10: Excess pore pressure presentation for UESCC with 326 elements.

A.2.2 Various rates and mesh densities

Results are obtained for fine, medium and coarse mesh quality and presented in Figure A.11, A.12 and A.13, respectively. All graphs indicates that increased rates will result in higher peak-values. It can also be seen a skewness for reduced mesh qualities. Peak-values slightly differs as 1400 compared to 326 element mesh quality differs with a maximum of 10 kPa.

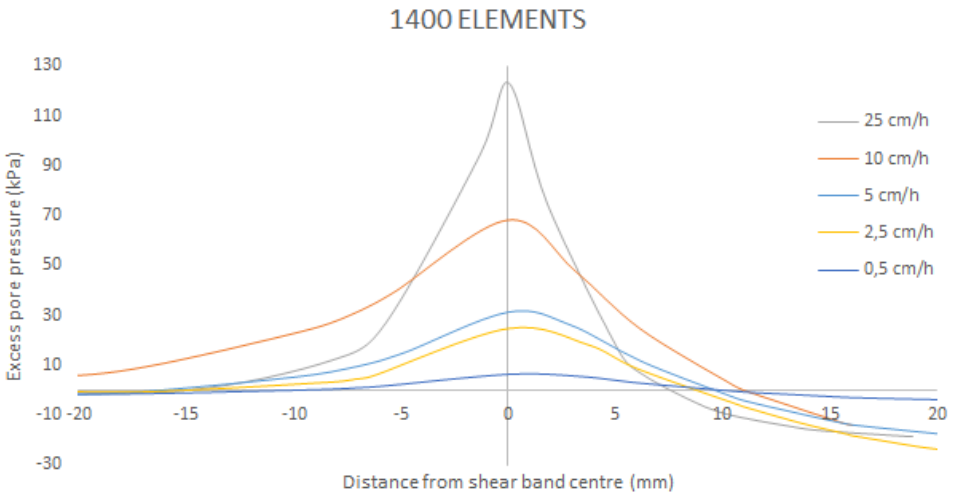

Figure A.11: Excess pore pressure distribution for the same time-step with various rates and 1400 element mesh refinement for UESCC model.

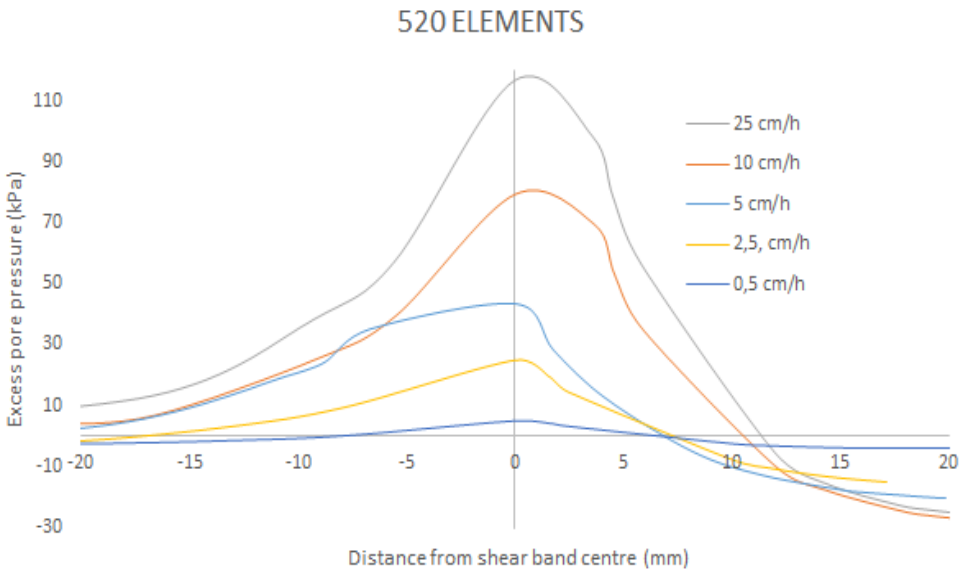

Figure A.12: Excess pore pressure distribution for the same time-step with various rates and 520 element mesh refinement for UESCC model.

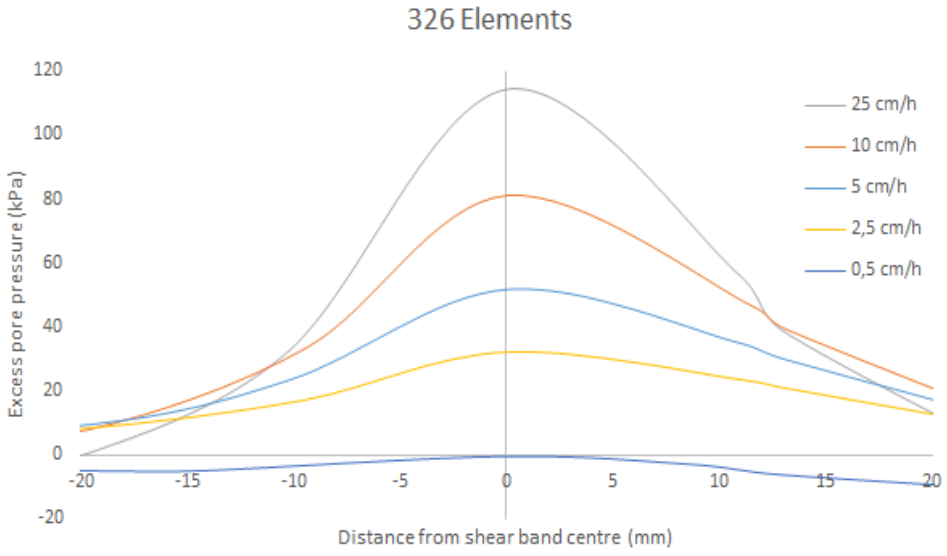

Figure A.13: Excess pore pressure distribution for the same time-step with various rates and 326 element mesh refinement for UESCC model.

Appendix B

Torque with various rates

This appendix contains further results from FEM regarding required torque for various rates with coarse, medium and fine mesh quality for HS and UESSC soil model.

B.1 Hardening soil

The mesh densities presented here are of fine(Figure B.1), medium(Figure B.2) and coarse(Figure B.3) quality. Results from fine and medium mesh are more or less similar with peak-values for faster rates of about 3.5-3.7 Nm. It can be observed that the coarse mesh differs significantly because of the scattering peak-strengths and the uplift in strength at further rotation.

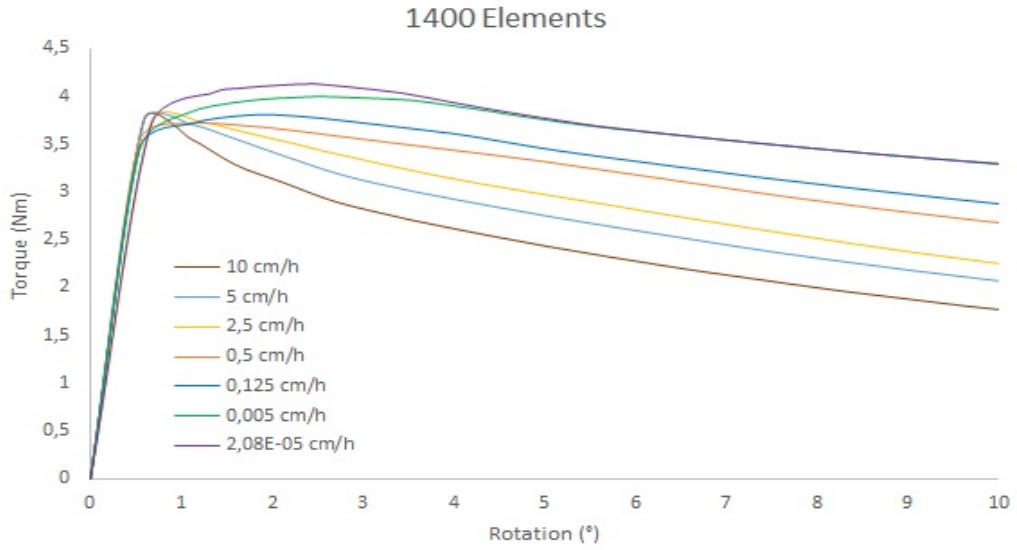

Figure B.1: Torque/rotation relation for HS with 1400 elements for various rates.

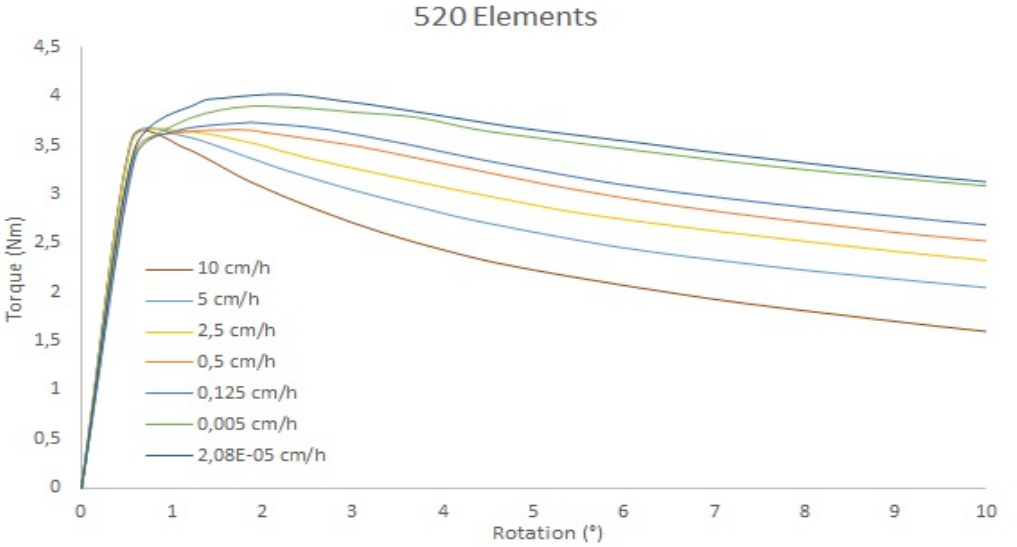

Figure B.2: Torque/rotation relation for HS with 520 elements for various rates.

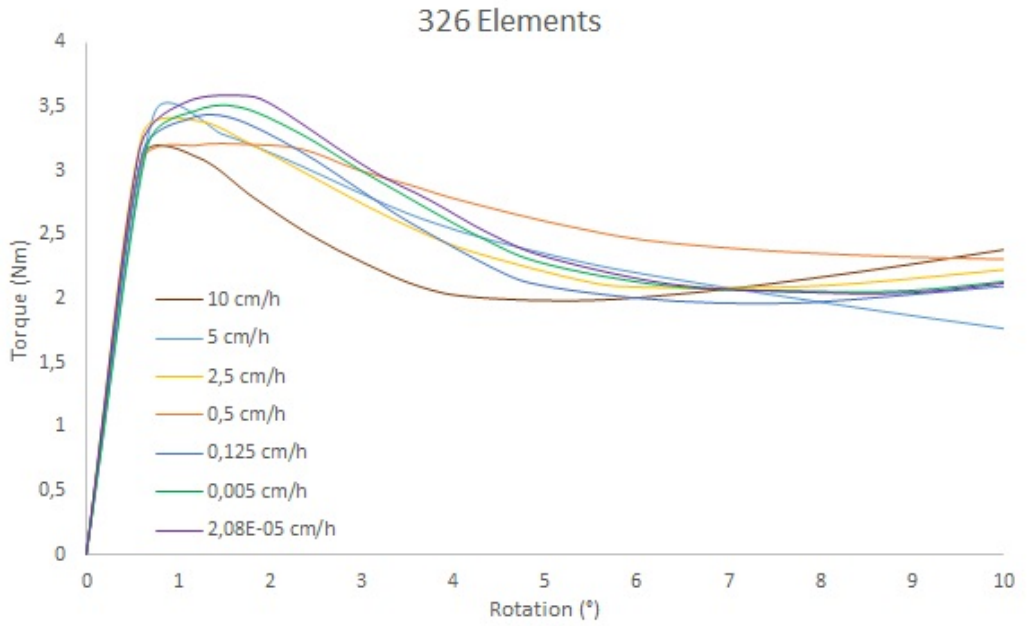

Figure B.3: Torque/rotation relation for HS with 326 elements for various rates.

B.2 Unified enhanced soft clay creep

Fine, medium and coarse mesh are presented in Figure B.4, B.5 and B.6, respectively. For mesh densities higher than 326 elements, issues regarding divergence during calculation can be seen as the curves stops at different rotation steps. This is more common for slower rates. Upon the investigation of mesh dependency with UESSC model, it can be seen that all the meshes refinements results in very similar outputs, although the results are non-unique.

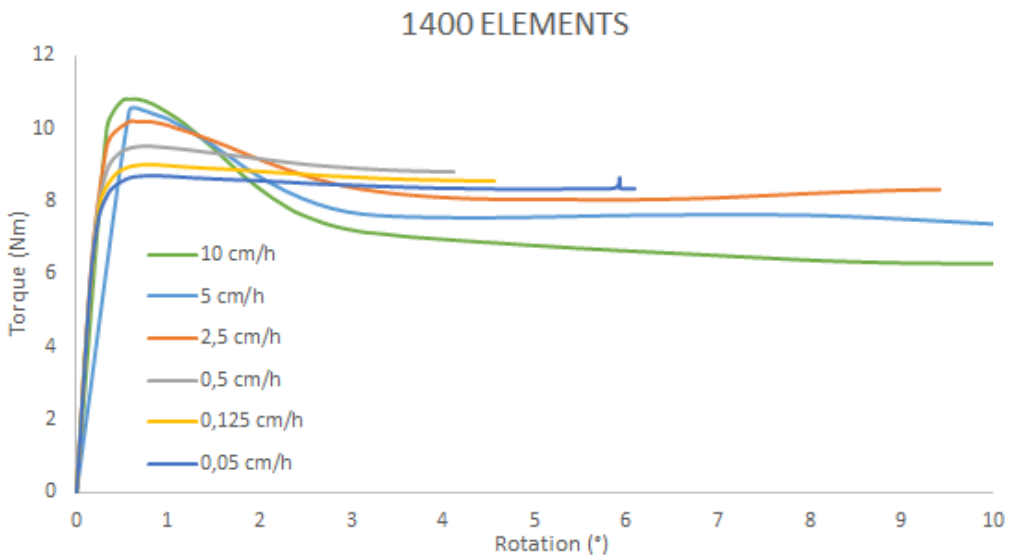

Figure B.4: Torque/rotation relation for UESCC with 1400 elements for various rates.

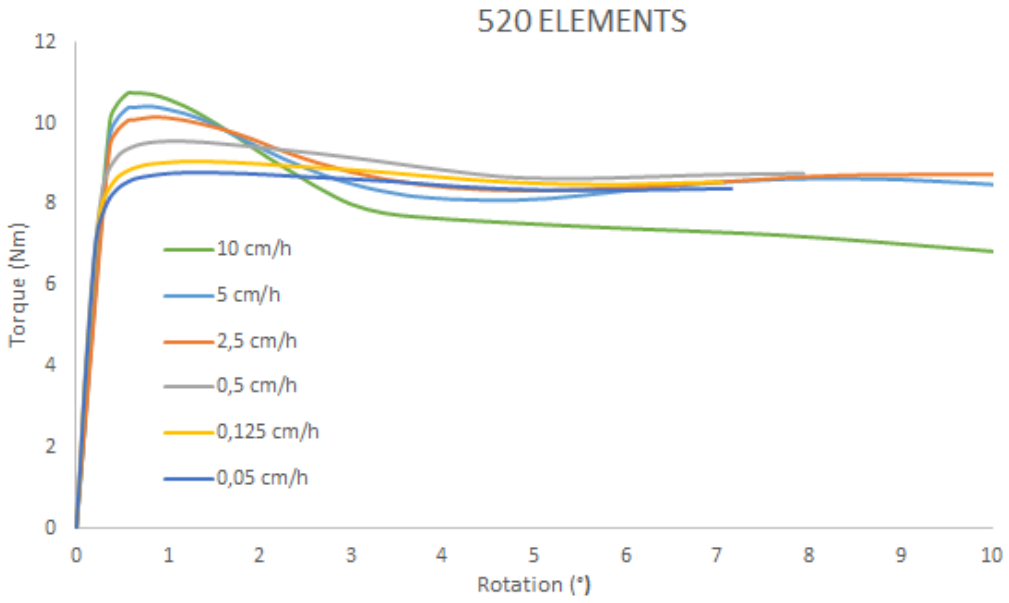

Figure B.5: Torque/rotation relation for UESCC with 520 elements for various rates.

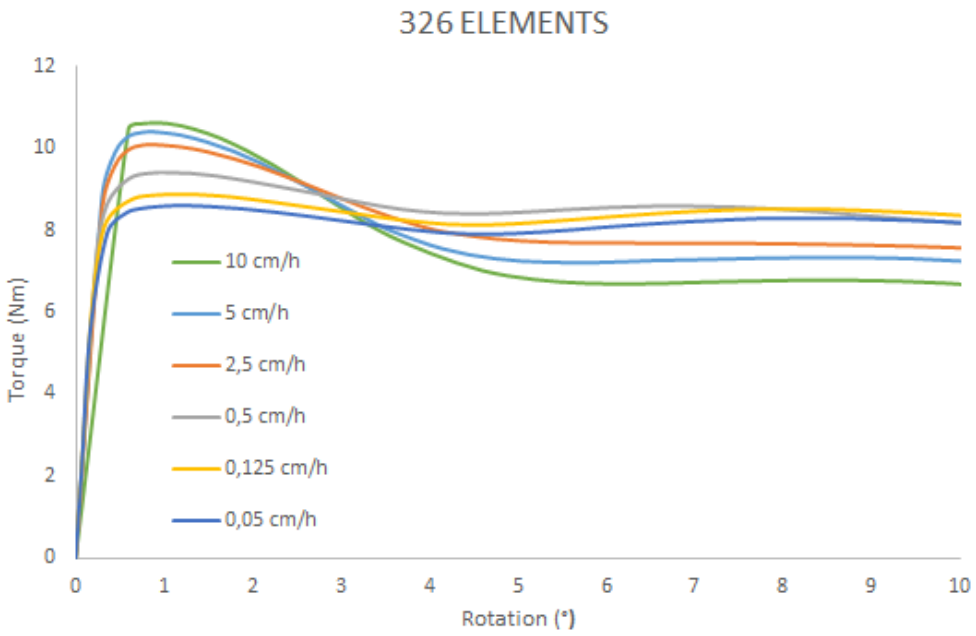

Figure B.6: Torque/rotation relation for UESCC with 326 elements for various rates.